Results in Engineering 30 (2026) 110820

Contents lists available at ScienceDirect

Results in Engineering

journal homepage: www.sciencedirect.com/journal/results-in-engineering

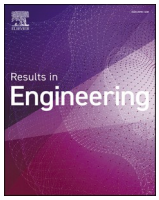

Research paper

An assessment of the performance of centrifugal screw pumps operating in reverse as turbines: A solution for fish-friendly micro-hydropower and pumping

Naufal Riyandi [a,*], John Gallagher [a], Rodolfo Espina-Valdés [b], Aonghus McNabola [c]

[a] Department of Civil, Structural & Environmental Engineering, Trinity College Dublin, Dublin, D02 PN40, Ireland
[b] Cuida, University of Oviedo, Gonzalo Gutiérrez Quirós St, 33600, Mieres, Spain
[c] School of Engineering, RMIT University, 124 La Trobe St, Melbourne, VIC 3000, Australia

ARTICLE INFO

Keywords:
Hydropower
Fish-friendly
Nature restoration
Pump-as-turbine
Computational fluid dynamics

ABSTRACT

The European Union's Nature Restoration Regulation (NRR) aims to restore ecosystems, including reconnecting 25,000 km of rivers by 2030 through barrier removal/modification. However, it also poses a significant challenge to micro-hydropower (MHP) development as barriers are crucial for run-of-river MHP systems and modifying them involves high costs. A promising synergistic solution is the use of centrifugal screw pumps (CSP) as fish-friendly turbines, allowing energy generation while maintaining river connectivity. However, their performance in turbine mode remains unknown. This study investigated CSP-as-turbines (CSPAT) performance using theoretical and numerical approaches including Computational Fluid Dynamics (CFD) analysis, and new one-dimensional (1D) prediction equations. Two small CSPs, CSP-1 and CSP-2, were first analysed, showing peak efficiencies of 22.8% and 28.7% at 800 RPM, respectively. To enhance performance, a larger model, CSP-3, was assessed, achieved 33.1% efficiency and 12.5 kW output at 32.2 m head and 120 l/s flow. Based on the CFD results, new 1D pump-to-turbine prediction equations were developed, demonstrating low prediction errors ($\leq$1.18%) and high accuracy ($R^2 = 0.979$ for relative head and $R^2 = 0.973$ for relative power). These findings enable the design of CSPAT for sustainable hydropower, pumping applications, and barriers modifications as part of nature restoration initiatives.

1. Introduction

Research has increasingly highlighted the importance of nature restoration to address recent declines in biodiversity worldwide, and as an effective means of both climate adaptation and mitigation [1]. Nature restoration is a wide-ranging activity covering land and water ecosystems. This activity includes restoring biodiverse habitats, increasing populations of beneficial insects, aiding wildlife recovery by expanding their ranges, expanding urban green spaces and tree cover, raising the share of farmland with diverse natural features, rehabilitating degraded peatlands, controlling invasive species, restoring coastal and marine ecosystems with iconic species, and improving and restoring freshwater ecosystems [2–4]. In response to this challenge, the European Union implemented the Nature Restoration Regulation (NRR) in 2024 [5]. This regulation includes provisions that require the preservation of aquatic ecosystems, both marine and freshwater. Additionally, it mandates the maintenance of river connectivity in Europe for up to 25,000 km by 2030 through the removal or modification of existing barriers [6].

However, it should be noted that the process of barrier removal or modification is complex and costly. Taking the small EU country of Ireland for example, >74,000 potential barriers have been identified, and the removal or modification of 257 of these has been targeted by 2027 [7]. Barrier removal or modification requires the execution of, and favourable outcomes from, up to eleven regulatory surveys. These include land, hydraulic, hydro-morphological, NIS, architectural, archaeological, underwater archaeological, pearl mussel and contaminated sediment surveys [8].

In addition to these, the issue of adjacent land and barrier ownership/access, and public opposition to change, add additional substantial challenges to policy implementation. Taken together the cost of individual barrier removal and the time required are both significant, with cost estimates of €250–500k per barrier [9]. Achieving the highlighted

* Corresponding author.
E-mail address: riyandin@tcd.ie (N. Riyandi).

https://doi.org/10.1016/j.rineng.2026.110820
Received 15 January 2026; Received in revised form 13 March 2026; Accepted 30 April 2026
Available online 30 April 2026

NRR targets amounts to a very significant total cost as a result. Therefore, solutions are required which could ease the financial burden of barrier modification, and time requirements for achieving nature restoration.

While the NRR is essential for the sustainability of aquatic ecosystems, it could also significantly challenge current and future run-of-river (RoR) micro-hydropower (MHP) systems, as existing barriers are critical elements of these systems, especially for increasing water surface levels that feed the intake. Many previous hydropower installations on a micro-scale have been incorporated into pre-existing river barriers, such as weirs or small dams to lower costs and avoid the environmental impacts of new barrier construction [10,11]. Therefore, removing or modifying barriers as part of the NRR could impact future RoR MHP resources and development.

Meanwhile, the utilisation of MHP plays a vital role in enhancing renewable energy penetration to meet the European Union's target of 42.5% renewable energy by 2030 [12]. MHP offers a low-emission solution that can address the intermittency issues associated with other renewable sources like wind and solar [13]. However, conventional hydropower technologies, especially turbines, can have negative environmental impacts, particularly harming aquatic life such as fish [14,15]. Conventional turbines such as Francis and cross-flow turbines are associated with particularly high fish mortality, which in some cases can exceed 90%. This conflict underscores the need for innovative solutions that align with the NRR's objectives while supporting sustainable energy development for climate adaptation and mitigation. Policies supporting nature restoration and the energy transition both aim to address the climate crisis, but this requires synergistic solutions to mitigate the aforementioned conflicts.

In response to these conflicts, especially ecological concerns, several hydropower technologies have been developed to improve fish survival rate, reduce injury, facilitate migration, and maintaining high passage efficiency, known as fish-friendly turbine technology [14,16–18]. Modification to conventional turbines, such as redesigning Kaplan turbine impellers, have seen some success but often result in increased cost and reduced hydraulic performance [19]. Alternative fish-friendly turbines, including Archimedes Screw Turbine (AST) and Very Low Head (VLH) turbines, have demonstrated low fish mortality rates of up to 8% [20,21]. However, both technologies face notable limitations: ASTs are constrained by maximum flow capacity, while VLH turbines are susceptible to cavitation and present logistical challenges related to transportation and installation [22].

To reconcile the dual objectives of nature restoration and renewable energy expansion, there is a clear need for a performant, cost-effective, environmentally compatible, and fish-friendly hydropower solution. One promising approach is the development of fish-friendly Pump-as-turbine (PAT) at MHP scale. PAT technology has been widely investigated in recent years as a low-cost and economically viable solution for MHP application [23]. Comparing with conventional turbines, PATs are less expensive and their components are market ready [23]. PAT research has focused heavily on developing methods for accurate prediction of PAT performance from known pump performance data [24]. These methods have relied on experimentation, developing analytical prediction methods, and using computational fluid dynamics [25,26]. However PAT research has also mostly focused on the reserve operation of single-stage centrifugal pumps given their wide range of applicability to different head and flow ranges. Developments focusing on other forms of pump working as turbines are less widespread, and the operation of fish-friendly PATs have been neglected to date.

Fish-friendly PATs could be crucial to future MHP developments in existing barriers as part of a barrier modification. Conventional PATs are unsuitable as these pose risks to fish survival. Fish passing through conventional pumps can face injury and mortality rates as high as 74% [27]. However, using a fish-friendly PAT could allow existing barriers to be modified allowing upstream transport of fish using a fish-friendly pump, and downstream fish-friendly generation of energy in reserve mode.

One fish-friendly pump that could be utilised as a turbine is the centrifugal screw pump (CSP). The CSP combines centrifugal pump principles with a screw-shaped impeller. This design allows it to transport live fish with low mortality [28,29]. The CSP has been shown to result in a minimal ratio of injuries lower than 3%, while pumping 2300 eels [30]. It has also been shown to result in no latent mortality on fish. Additionally, another experiment was carried out to assess the level of fish friendliness of CSPs by passing juvenile fish, larvae, and fish eggs through it. The results found that >99% of the test subjects managed to successfully pass through the CSP and were retrieved with no injuries, which was also confirmed after 48 h [31]. In reverse as a PAT the CSP could also offer fish-friendly MHP production as part of barrier modification. However, research investigating the performance of centrifugal screw PATs is lacking, and their performance in this role remains unexplored. This study provides the first comprehensive analysis of centrifugal screw PAT (CSPAT) performance using two approaches: Computational Fluid Dynamics (CFD) analysis and one-dimensional (1D) equations. The results from experimentally validated CFD analysis and 1D analysis were compared to develop predictive equations that simplify performance estimation for CSPATs without requiring further simulations or experiments, thereby reducing both cost and time investment. This research is the first to investigate the performance of centrifugal screw PATs using CFD, filling a critical gap in the existing literature.

2. One-dimensional analysis

The performance of the CSPAT, which remains unknown, could be predicted using existing 1D equations as a theoretical approach. The 1D analysis offers a cost-effective alternative to experimental testing or computationally intensive CFD simulations [32]. These existing 1D equations were developed based on the pump's Best Efficiency Point (BEP) in reverse mode [32–35]. However, pump manufacturers often do not provide the BEP in turbine mode due to cost constraints [32]. Therefore, an alternative approach is needed to estimate the BEP in turbine mode using data from pump mode. Yang et al. [36] developed the following theoretical equations to predict the PAT's BEP based on its BEP in pumping mode, as shown in Eqs. (1–4).

$$H_t = hH_p \tag{1}$$

$$h = \frac{1.2}{\eta_p^{1.1}} \tag{2}$$

$$Q_t = qQ_p \tag{3}$$

$$q = \frac{1.2}{\eta_p^{0.55}} \tag{4}$$

In this context, H_t refers to the head when operating as a turbine (m), while H_p is the head when operating as a pump (m). The variable h represents the ratio between the head in turbine and pump modes. η_p denotes the efficiency when the unit operates as a pump. Q_p is the flow rate when functioning as a pump (m^3/s), and Q_t is when operating as a turbine (m^3/s). The variable q represents the ratio between the flow rate in the turbine and pump modes.

Meanwhile, to estimate the rotational speed in turbine mode, based on the measured pump mode performance, Eqs. (5) and (6), developed by Fontanella et al. [37] can be used.

$$N_t = \frac{N_p}{1.3595}\frac{Q_{tb}}{Q_{pb}} \tag{5}$$

$$P_{tb} = P_{pb}\left(\frac{N_t}{N_p}\right)^3 1.0403 \tag{6}$$

Table 1
Coefficients values for predicting conventional PAT characteristics using Eqs. (8) and (9).

Non-dimensional head curve		Non-dimensional power curve	
Coefficients	**Values**	**Coefficients**	**Values**
a	1.160	d	1.248
b	$(0.0099\ N_s + 1.2573) - 2a$	e	$(0.0108\ N_s + 2.2243) - 2d$
c	$1 - a - b$	f	$1 - d - e$

Table 2
CSPAT BEP in pumping mode.

	Pump Type	
	CSP-1	CSP-2
Flow Rate (m^3/s)	0.0125	0.0158
Head (m)	4.6	4.8
Power (W)	1020	1310
Pump Efficiency	0.542	0.580
Rotational Speed (RPM)	1445	1455

Where N_t represents the rotational speed when operating as a turbine (rad/s), and N_p is the rotational speed when operating as a pump (rad/s). Q_{tb} refers to the flow rate at the Best Efficiency Point (BEP) in turbine mode (m^3/s), while Q_{pb} is the flow rate at the BEP in pump mode (m^3/s). P_{tb} is the power generated at the BEP when operating as a turbine (W), and P_{pb} is the power required by the pump at the BEP (W).

Additionally, to calculate the specific speed (N_s), one of necessary parameters for estimating the performance of a PAT, Eq. (7) can be used.

$$N_s = N\left(\frac{\sqrt{Q_{BEP}}}{H_{BEP}^{3/4}}\right) \tag{7}$$

The characteristics of the PAT can be predicted using a theoretical approach developed by Novara et al. [33], which was based on data from 113 pumps of various sizes and manufacturers, including radial end-suction, semi-axial, and axial PATs. Novara's method [33] outlined in Eqs. (8) and (9), is capable of predicting conventional PAT characteristics with an R^2 of up to 0.9701 and a Root Mean Square Error of up to 0.0751.

$$\frac{H_t}{H_{tb}} = a\left(\frac{Q_t}{Q_{tb}}\right)^2 + b\left(\frac{Q_t}{Q_{tb}}\right) + c \tag{8}$$

$$\frac{P_t}{P_{tb}} = d\left(\frac{Q_t}{Q_{tb}}\right)^2 + e\left(\frac{Q_t}{Q_{tb}}\right) + f \tag{9}$$

Where H_{tb} refers to PAT's head at the BEP (m), P_t refers to power of the PAT (W). Meanwhile, the values of coefficients a through f are provided in Table 1.

The efficiency of the PATs (η_t) can be predicted by using Eq. (10), where P_t refers to PAT power in kW, and g refers to gravity (9.81 m/s^2) [33].

$$\eta_t = \left(\frac{P_t}{H_t Q_t g}\right) \tag{10}$$

In addition to [33], several other methods have been developed by researchers. Fecarotta et al. [38] proposed a method to predict the performance of PATs, as presented in Eqs. (11) and (12). This method demonstrated good accuracy, with mean errors of up to 0.0393 for head, 0.0793 for power, and 0.0252 for efficiency [38]. However, the Fecarotta method is only applicable within a specific speed range of around 120 to 162 [38]. Moreover, it was originally developed for semi-axial pumps in the first stage, which means the results may vary when applied to other types of pumps or different specific speed ranges [38].

$$\frac{H_t}{H_{tb}} = 1.61\left(\frac{Q_t}{Q_{tb}}\right)^2 - 1.41\left(\frac{Q_t}{Q_{tb}}\right) + 0.805 \tag{11}$$

$$\frac{P_t}{P_{tb}} = 1.85\left(\frac{Q_t}{Q_{tb}}\right)^2 - 0.858\left(\frac{Q_t}{Q_{tb}}\right) - 0.00567 \tag{12}$$

Another method was developed by Barbarelli et al. [35], who based their research on centrifugal pumps. The pumps used had specific speeds ranging from 5 to 65. The authors conducted laboratory experiments to develop predictive equations (Eqs. (13) and (14)) for PAT performance. The method showed an error of around 20% and an R^2 of 0.86 for the head coefficient characteristic, and about 15% error with an R^2 of 0.6 for the flow rate coefficient characteristic. Additionally, the error between theoretical and experimental efficiency was approximately 5%, with an R^2 of 0.9 [35].

$$\frac{H_t}{H_{tb}} = 0.922\left(\frac{Q_t}{Q_{tb}}\right)^2 - 0.406\left(\frac{Q_t}{Q_{tb}}\right) + 0.483 \tag{13}$$

$$\frac{P_t}{P_{tb}} = 0.040\left(\frac{Q_t}{Q_{tb}}\right)^3 + 1.185\left(\frac{Q_t}{Q_{tb}}\right)^2 - 0.043\left(\frac{Q_t}{Q_{tb}}\right) - 0.183 \tag{14}$$

Barbarelli et al. [35] also developed an equation to predict efficiency, as shown in Eq. (15), where η_{tb} refers to PAT efficiency at BEP. Since efficiency is calculated from the predicted head and power, this equation enables the evaluation of overall PAT performance. Although the head and flow coefficient errors are relatively higher, the small efficiency error indicates that the mofel remain suffucuently reliable for system-level performance prediction.

$$\eta_t = \left(\frac{P_t/P_{tb}}{(H_t/H_{tb})(Q_{tb})}\right)\eta_{tb} \tag{15}$$

In this study, the correlations proposed by Yang et al. [36]] and Fontanella et al. [37] were used to estimate the turbine-mode BEP based on the pump-mode BEP data. The predicted turbine BEP values were then used as input to evaluate turbine performance using the methods developed by Novara et al. [33], Fecarotta et al. [38], and Barbarelli et al. [35]. The pump data employed in this work correspond to manufacturer test result at the BEP in pump mode for centrifugal screw pumps. These data were directly obtained from the manufacturer and were not derived from any averaged experimental database.

2.1. CSPAT characteristics in pumping mode

Two types of pumps, referred to as CSP-1 and CSP-2, were analysed in reverse mode. These pumps' feature V-type closed impeller pumps, designed specifically to operate under abrasive conditions and to accommodate flow streams containing materials such as sand sediment, and biological particles, including fish [39]. Additionally, this design characteristic makes the pumps particularly suitable for low-head riverine micro hydropower applications, where environmental considerations and debris-laden flow are commonly encountered. The selection of these two pump models was also based on the availability of manufacturer performance data. The BEP values for both types in pumping mode have been provided by the manufacturer, as shown in Table 2. Furthermore, a view of V-type closed impeller can be seen in Fig. 1. Both of CSP-1 and CSP-2 featured the same shape impeller.

2.2. Best efficiency point of CSPAT

Eqs. (1) through Eq. (7) were used to predict the CSPAT's BEP based on its BEP in pumping mode. Subsequently, the head in turbine mode at BEP condition, along with the head and efficiency in pumping mode at the BEP, as demonstrated in Table 2, were entered into Eqs. (2) and (1). Additionally, the flow rate and efficiency in the pumping mode were substituted for the turbine mode flow rate in Eqs. (4) and (3). In order to

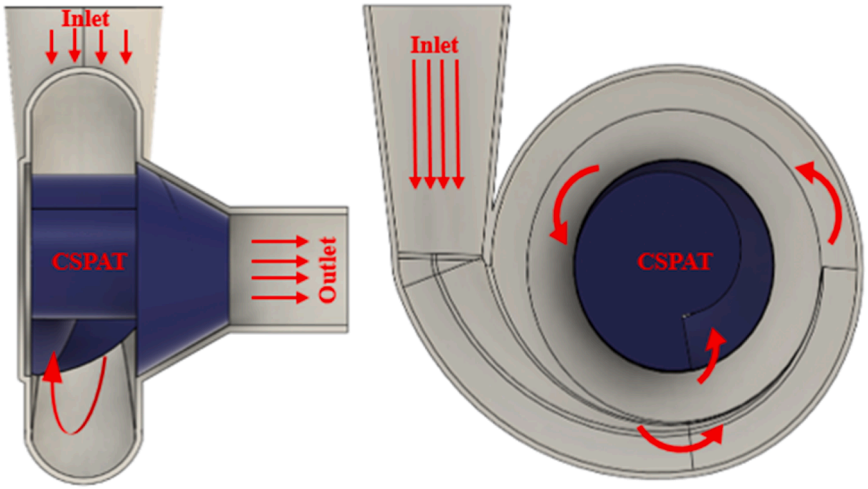

Fig. 1. CSPAT model for V-type closed impeller.

Table 3
BEP of CSPAT.

Type	Flow Rate (m^3/s)	Head (m)	Power (W)	Efficiency (η_p)	Rotational Speed (RPM)	Specific Speed (N_s)
CSP-1	0.02101	10.83	2005	0.9002	1786	43.38
CSP-2	0.02558	10.49	2302	0.8766	1733	47.56

calculate the rotational speed, Eq. (5) was utilised, with the flow rate and rotational speed in pumping mode as well as the turbine mode flow rate from the previous calculation being substituted. To calculate the power in turbine mode at the BEP, Eq. (6) was employed. This calculation involved substituting the power and rotational speed in pumping mode at the BEP, as well as the rotational speed in turbine mode, which was subsequently calculated. The specific speeds in turbine mode at the BEP were derived by substituting the result of the head, power, and rotational speed at BEP calculation into Eq. (7). Finally, the efficiency in turbine mode at the BEP was determined through a comparative analysis of power at the BEP, as determined by calculation, and multiplication of flow rate at BEP, head at BEP water density and gravity. The results are presented in Table 3.

Based on the existing methodology, the flow rate and head at the BEP of the CSP-1 and CSP-2 theoretically increase when operated as a turbine. This finding is consistent with research conducted by Yang et al. [40], Raman et al. [41], and Yang et al. [36] which compared the BEP performance of centrifugal pumps in both pump and turbine modes. These increases indicate that to reach the peak performance in turbine mode, the flow rate and head must be increased compared to their peak values in pump mode. The increase in flow rate and head theoretically also lead to higher output power and efficiency of the CSPAT, which aligns with the findings of Yang et al. [40] for their centrifugal PAT. However, other studies conducted by Raman et al. [41] and Yang et al. [36], show that both power and efficiency of the centrifugal PAT decrease compared to pump mode. This decline is attributed to additional losses resulting from a change in function and flow direction within the pump. For this reason, a CFD simulation is needed to confirm the performance of CSPAT.

2.3. CSPAT characteristic using 1-D analysis

The characteristic of the CSPAT for CSP-1 and CSP-2 can be predicted using equations from Eqs. (8–14). The results can be observed as shown in Figs. 2 and 3 for the head, power and efficiency curves, respectively.

Based on Fig. 2, CSP-1 is predicted to produce a higher head at lower flow rates compared to CSP-2. This indicates that CSP-1 more effectively converts kinetic energy into potential energy, particularly at flow rates exceeding 20 l/s. Consequently, CSP-1 is predicted to be better suited for applications requiring higher heads than CSP-2. However, at flow rates below 20 l/s, CSP-2 is predicted to hold greater stability compared to CSP-1.

Among the three methods analysed, Fecarotta et al. [38] predicts a

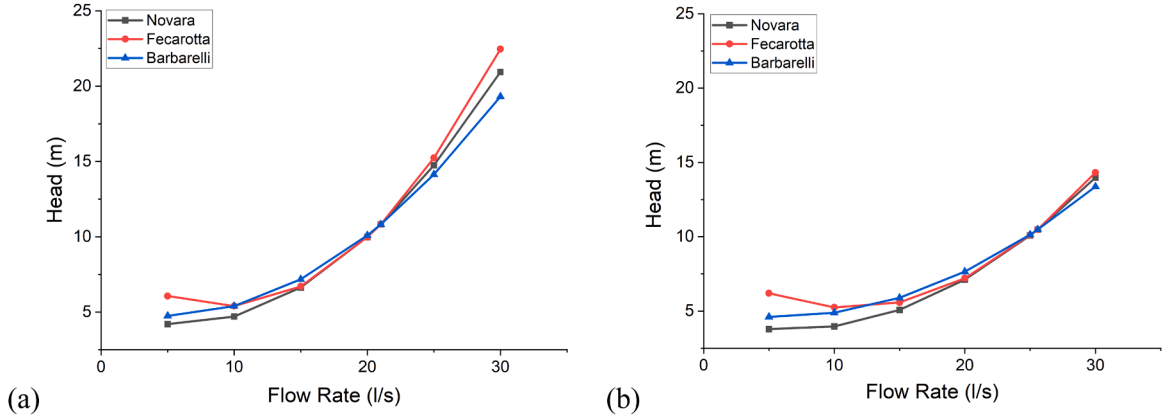

Fig. 2. Head curve of CSPAT based on existing 1-D analysis: (a) CSP-1; (b) CPS-2.

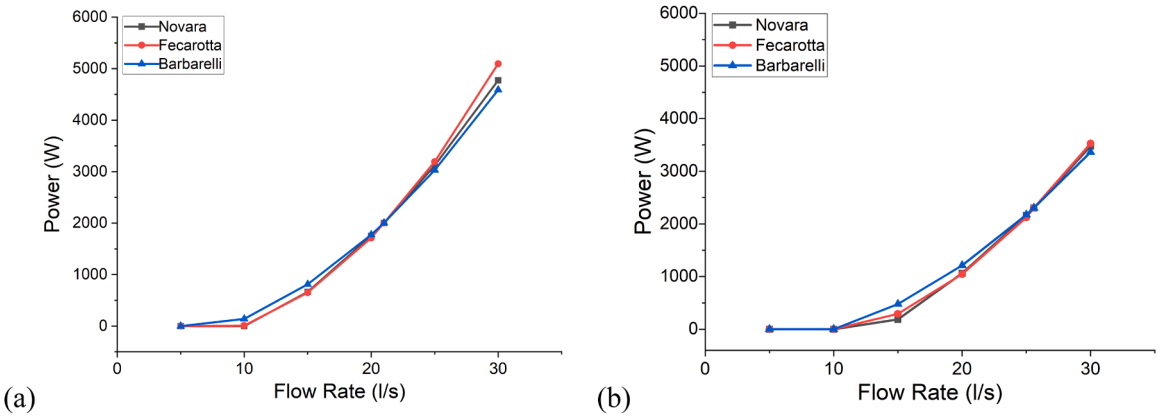

Fig. 3. Predicted power curve of CSPAT based on existing 1-D analysis methods: (a) CSP-1; (b) CSP-2.

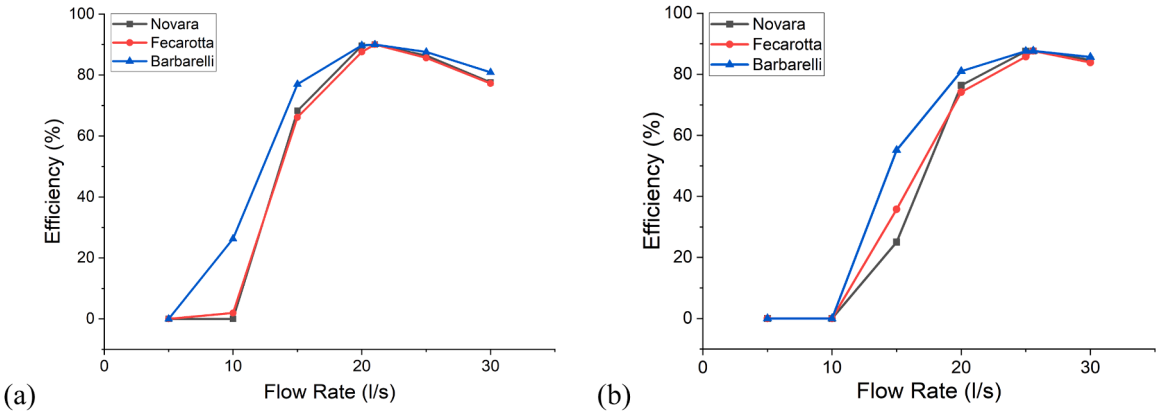

Fig. 4. Predicted efficiency curve of CSPAT based on existing 1-D analysis methods: (a) CSP-1; (b) CSP-2.

progressively increasing head as the flow rate rises, especially beyond the BEP. In contrast, Barbarelli et al. [35] predicts higher head values at mid-range flow rates (below BEP) but yields the lowest values when the flow rate exceeds the BEP. Meanwhile, Novara et al. [33] head predictions are lower than both Fecarotta et al. [38] and Barbarelli et al. [35] at flow rates below the BEP. Overall, the head increments predicted by Barbarelli and Novara are more stable than those of Fecarotta.

Fig. 3 presents the power curves of the CSPATs and shows how CSP-1 is predicted to generate higher power output than CSP-2, which aligns with the previous head results. Since CSP-1 produces a higher head, it also delivers greater power compared to CSP-2. This suggests that CSP-2 is better suited for applications with lower head and higher flow rates, while CSP-1 performs optimally under higher-head, low-flow conditions.

Regarding the three methods, Barbarelli et al. [35] predicts higher power than the other two methods at flow rates below the BEP, but its predictions become the largest after the BEP. In contrast, the Fecarotta et al. [38] method predicts the lowest power below the BEP and the highest beyond it, particularly for CSP-1. Meanwhile, the Novara et al. [33] method shows relatively stable power increments for both pump types across all flow rates.

Fig. 4 suggests that CSP-1 tends to achieve higher efficiency at the BEP compared to CSP-2. Additionally, CSP-1 is predicted to maintain relatively higher efficiency at flow rates below the BEP. However, beyond the BEP, CSP-1′s efficiency is predicted to decrease more sharply than CSP-2′s. CSP-2 is predicted to demonstrate greater stability at higher flow rates, as its post-BEP efficiency decline seems to be more gradual. These observations suggest that CSP-1 may perform more efficiently under low-flow, high-head conditions, while CSP-2 could be more suitable for high-flow applications.

Among the three evaluation methods, Barbarelli et al. [35] appears to predict the highest efficiency values, which may indicate a tendency towards more optimistic estimates relative to the other methods. The Fecarotta et al. [38] method tends to yield lower efficiency predictions at low flow rates, particularly for CSP-1, but shows a notable increase at higher flow rates. In contrast, the Novara et al. [33] method appears to produce more consistent results, with less pronounced efficiency variations across different flow rates.

The sensitivity of each method can be evaluated using Figs. 5 and 6. The method by Novara et al. [33] shows a less steep and more gradual gradient compared to the others. Meanwhile, the Fecarotta et al. [38] method displays the steepest gradient, which may indicate potential overfitting. The Barbarelli et al. [35] method shows smoother transitions than the other two, but because it has the smoothest surface of all three, it may tend to underestimate values. When there are changes in the N_s, the Novara method demonstrates the most gradual and relatively linear response. In contrast, the Fecarotta et al. [38] method shows the steepest transition with N_s variations, while Barbarelli et al. [35] produces the flattest and most linear changes.

Therefore, the Fecarotta et al. [38] method is most sensitive to N_s variations, Novara remains relatively stable, and Barbarelli et al. [35] is the least sensitive. As a result, Novara et al. [33] appears most suitable for preliminary CSPAT design estimation. However, it's important to note that all these existing methods were developed for performance prediction of conventional PATs, not specifically for CSPATs. To properly assess the accuracy of these 1-D analysis predictions for CSPAT characteristics, validation through laboratory experiments or numerical CFD analysis is required. This study focuses on an experimentally validated CFD-based comparison.

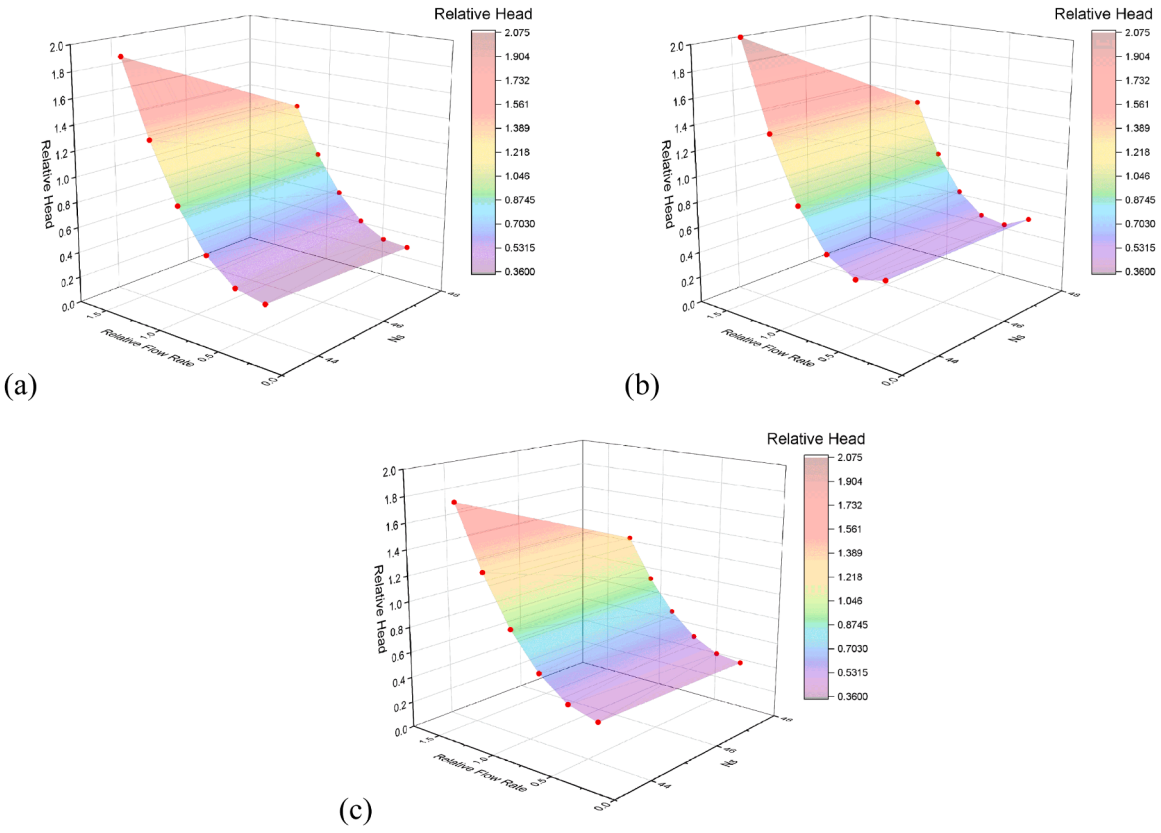

Fig. 5. Curves of relative flow and head to Ns: (a) Novara; (b) Fecarotta; (c) Barbarelli.

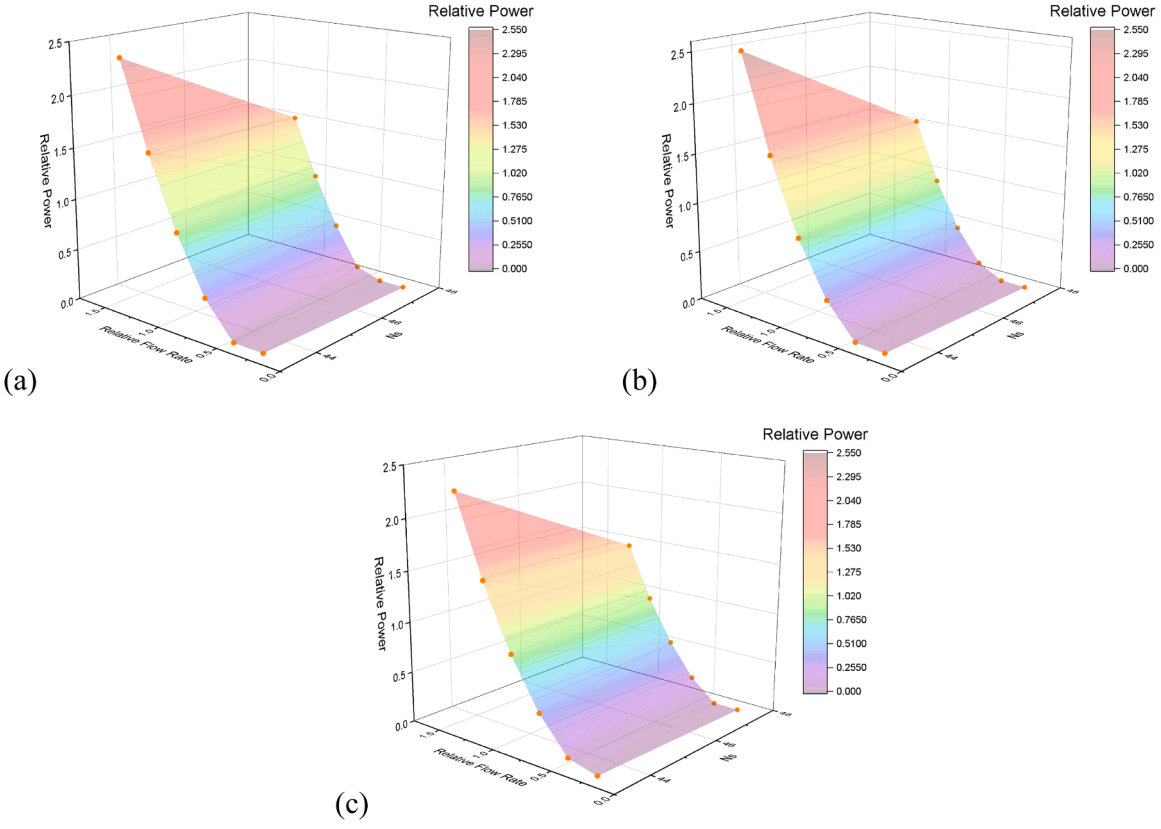

Fig. 6. CSPAT Curves of relative flow and power to Ns: (a) Novara; (b) Fecarotta; (c) Barabrelli.

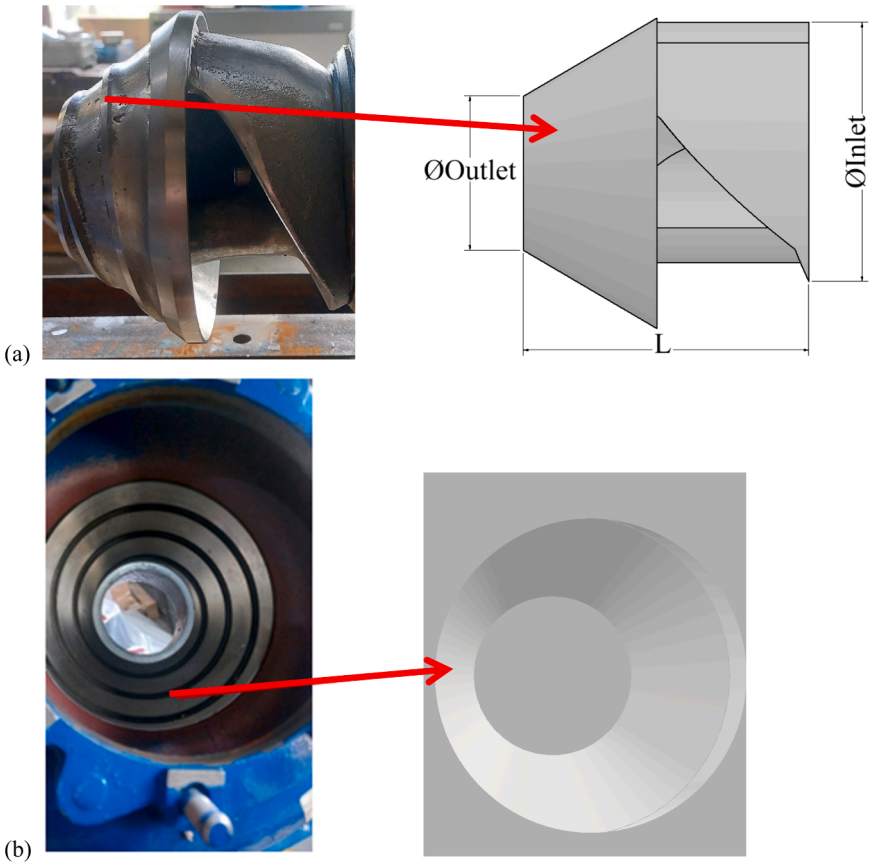

Fig. 7. Geometry simplification: (a) Surface screw on the impeller cone; (b) Surface screw on the volute cone.

Table 4
CSPAT dimension.

Parameters	CSP-1	CSP-2
$Ø_{Out}$ (cm)	7.5	7
$Ø_{In}$ (cm)	15	17.5
L (cm)	15	15.5

3. Numerical methods

In this study, CFD analysis was performed to examine the operation of CSPs in both pumping and reverse (turbine) modes. The simulation in pumping mode is essential, as it provides a benchmark for validation using existing experimental performance data—thereby ensuring the model's capability to accurately replicate real-world behaviour [42,43]. If the model validation yields an error margin of <10%, the CFD model is deemed sufficiently reliable to be employed in predicting reverse-mode performance [43]. In this context, the CFD results are used to evaluate the performance of CSPs operating in reverse mode and are further compared with predictions derived from established one-dimensional theoretical models.

3.1. Modelling

A 3D model of the fluid domain of the CSPAT was created, including components such as the volute, impeller, and inlet and outlet pipes. The volute and piping were modelled in Autodesk Inventor Professional 2023, while the screw impeller was designed in Autodesk Fusion 360 for greater flexibility in screw design. CFD model geometry was based on the measurement of dimensions of commercially available CSPs, while some simplifications were made to the modelled design to save on computational resources. These simplifications involve the cone surfaces of the impeller and volute, where the indented screw pattern was removed. This adjustment was made because there is no water flow in those areas, as shown in Fig. 7, allowing for easier meshing and simulation by reducing complexity.

Regarding size, the study uses small-sized machine of the CSP units as specified in Table 4. This selection was based on the pump's operational characteristics, which enable effective performance at low heads (4.5–5 m range) with flow rates between 12–16 l/s as specified also in Table 2.

The small-sized machine at full-scale configuration was chosen for three practical reasons: laboratory installation feasibility, initial testing convenience, and cost efficiency. Smaller units simplify initial examination and allow for easier performance evaluation. If initial results prove unsatisfactory, the small-sized data provides a reliable foundation for determining optimal larger-sized dimensions while minimising development costs.

3.2. Numerical analysis

In CFD, the Navier-Stokes equations are the foundation for solving fluid flow problems [44–46]. The Navier-Stokes equations used are the continuity equation (Eq. (16)) and the momentum conservation equation (Eq. (17)) [46].

$$\frac{\partial \rho}{\partial t} + \frac{\partial(\rho u)}{\partial x} + \frac{\partial(\rho v)}{\partial y} + \frac{\partial(\rho w)}{\partial z} = 0 \tag{16}$$

$$\frac{\partial(\rho \mathrm{u})}{\partial t} + \nabla.(\rho \mathrm{uu}) = -\nabla p + \frac{1}{Re}.\tau \tag{17}$$

Where ρ represents density (kg/m^3), t denotes time (s), u is the velocity vector (m/s) consisting of three directional components: u (x-direction), v (y-direction), and w (z-direction), all expressed in m/s. The coordinates

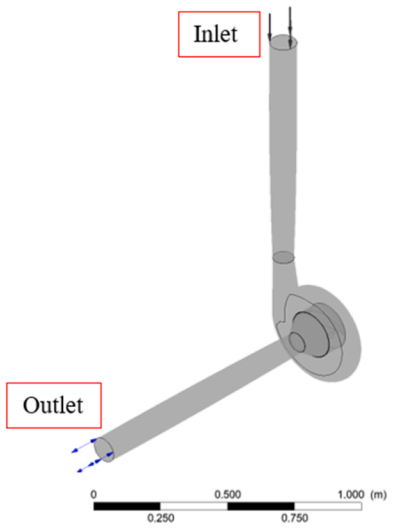

Fig. 8. Configuration of CFD domain with inlet and outlet locations.

x, y, and z correspond to the vector's spatial directions. Additionally, p represents pressure (N/m^2), Re is Reynold number, and τ refers to viscous stress tensor (N/m^2).

The Navier-Stokes equations can be solved using the unsteady Reynolds-Averaged Navier-Stokes (uRANS) approach, as this method can predict the global performance of the turbomachinery [47]. It Is evident that uRANS still commonly use in the numerical studies [48]. In comparison with alternative methodologies, Large Eddy Simulation (LES) has been demonstrated to predict more minutiae particularly with regard small vortices, than the uRANS [47]. However, it should be noted that LES approach necessitates a larger investment of both time and computational cost [47]. For that reason, the uRANS model was selected for this study. Furthermore, the mean performance of the turbomachinery must be considered. The mean performance prediction from the LES method does not enhance the quality of the uRANS method [49].

The study also utilised the RANS method at the commencement of the simulation to expedite the attainment of convergence conditions. This was accomplished by acquiring the initial value that would subsequently be employed in the transient simulation using uRANS [50]. RANS is a widely adopted method in numerical simulations due to its proven accuracy in modelling fluid behaviour within pumps and turbines [51]. This approach works by decomposing flow velocities into time-averaged and fluctuating components, allowing for efficient computation while maintaining reliable results in complex fluid dynamics scenarios [46].

$$\rho(\bar{u}.\nabla)\bar{u} = -\nabla\bar{p} + \mu\nabla^2\bar{u} - \nabla.(\rho\overline{u'u'}) \quad (18)$$

In formulation on Eq. (18), $\bar{u}$ refers to average velocity vector (m/s), $\bar{p}$ denotes the time-averaged pressure (N/m^2), μ represents viscosity (kg/m.s), and $\overline{u'}$ refers to time-averaged turbulent velocity fluctuations (m/s).

3.2.1. Turbulence model

The turbulence model that been used for this study is Shear Stress Transport (SST) model. The selection of the SST model was due to the SST turbulence model being a combination of the k-ω and k-ε models. For the flow near the wall, it is solved using the k-ω model, while for the flow far from the wall, it is solved using the k-ε model [52–54]. The SST model is also very good at estimating separated flow and swirl along walls with complex shapes [55]. Therefore, the SST model can work well for analysing complex flows in fluid machinery [56].

Additionally, the SST model was coupled with an automatic near-wall treatment to model turbulence in the vicinity of solid boundaries. This approach provides a smooth transition between low-Reynolds-number, wall-resolved behaviour, and wall-function-based formulations, depending on the local y^+ values and mesh resolution. The near-wall resolution was assessed through the non-dimensional wall distance y^+, yielding average values of 106.53 for CSP-1 impeller and 71.35 for CSP-2 impeller. These values fall within the recommended range for wall-function-based integration of the SST model, typically $30 < y^+ < 300$ [57–59]. This ensures that the first off-wall node lies within the logarithmic region of the boundary layer, maintaining consistency between the mesh resolution and the selected near-wall treatment. Consequently, the grid is adequate to capture the overall boundary-layer behaviour without resorting to fully resolved viscous-sublayer modelling.

3.2.2. Boundary condition

In the CFD analysis, Ansys CFX 2022 R1 was used. The computational domain was divided into two regions: a stationary domain and a rotary domain. The stationary domain consisted of the inlet and outlet pipes as well as the volute. The boundary conditions applied to the pipes included a mass flow rate at the inlet and a static pressure opening at the outlet. The mass flow rate values were varied from 5 to 30 kg/s, in six 5 kg/s intervals. The values were chosen based on previous studies, which reported that the flow rate in turbine mode increased by approximately 11–70% compared to pumping mode [40,41]. Furthermore, according to the calculations presented in Section 2.2, the BEP flow rate for the CSP-1 was expected to be 20.01 l/s, while the CSP-2 had a flow rate of 25.52 l/s. Additionally, a low flow rate was selected to observe how effectively the CSPAT can convert low flow conditions into usable power. The outlet pressure was set to atmospheric pressure, 1 atm. A no-slip wall condition was applied to the pipe and volute walls, with a wall roughness of 11 μm for the pipe and 45 μm for the volute. The configurations and the fluid direction from inlet to outlet can be observed in Fig. 8.

The rotary domain included the impeller, which was also assigned a no-slip wall condition with a wall roughness of 45 μm. For the rotational speed selection, analytical calculations in Section 2.2 yielded theoretical BEP speeds of 1786 RPM for CSP-1 and 1733 RPM for CSP-2. However, since the device needs to be fish-friendly, previous research [60–62] recommended operating at lower RPM. Higher rotational speed are associated with increasing rates of fish injuries. Additionally, higher rotational speed also increases the rate of collision of the fish with the partitions of the impeller as well as enhances the effect of suction which potentially impacts fish [14,63]. To account for potential real-world operation at significantly lower RPM, speeds were varied in this study from 300 to 1200 RPM.

3.3. Mesh convergence

The meshing process was carried out using ANSYS ICEM for the stationary domain, including volute, inlet and outlet pipes, and cone volute, utilising a blocking system, and ANSYS Mesh for the rotary domain, including impeller. The rotary geometry has a spiral shape and is more complex, requiring a more robust tetrahedral mesh. The fluid domains and the mesh configurations are shown in Fig. 9. To assess the accuracy of the mesh, a mesh convergence test was conducted. This test was performed to evaluate the stability of the simulation results concerning variations in mesh density [64].

Seven different mesh levels, ranging from coarse to fine grids, were tested under a representative condition. The mesh convergence studies were performed at a rotational speed of 500 RPM to represent the mid-range operating condition within the investigated speed range (300–1200 RPM). For each mesh level, the studies resulting torque and head values.

Based on the results of the convergence test shown in Fig. 10, when the mesh density increased, the value of both torque and head became more stable and consistence. The minimum number of elements required for the simulation was 1666,432 for CSP-1, consisting of

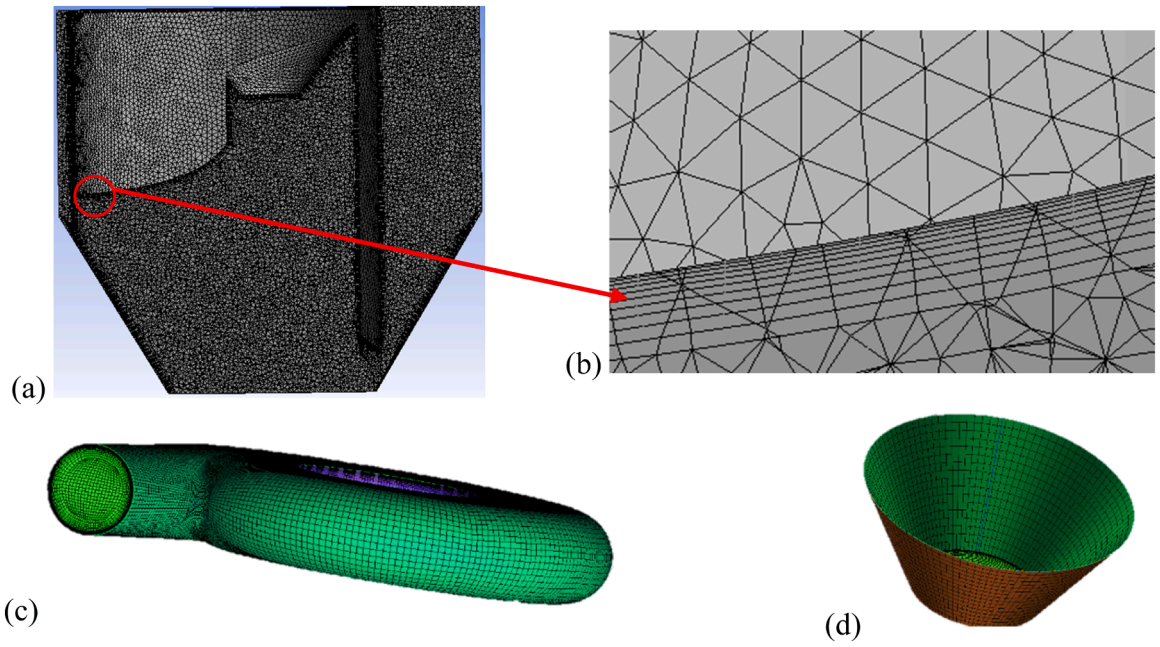

Fig. 9. Fluid domain mesh: (a) Cross-section impeller; (b) Inflation layer impeller; (c) Volute; (d) Cone volute.

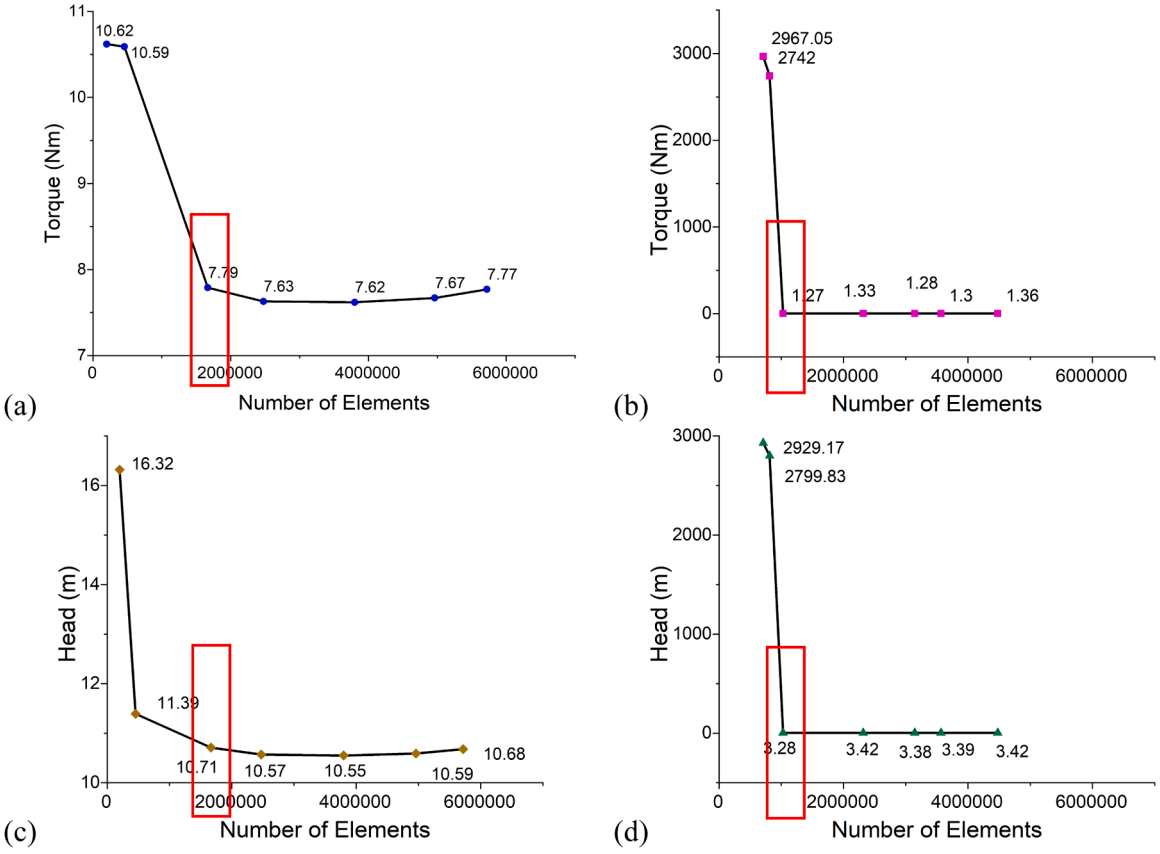

Fig. 10. Mesh convergence test results: (a) CSP-1 torque; (b) CSP-2 torque; (c) CSP-1 head; (d) CSP-2 head.

1386,588 elements in the stationary domain and 279,844 elements in the rotary domain. This mesh size was selected because the relative difference between successive refinements was below approximately 5%, indicating that further refinement produced only marginal changes in the predicted torque and head values. At this level, the torque ranged from approximately 7.6 to 7.8 Nm and the head varied between10.55 and 10.71 m under the condition of 500 RPM and 30 l/s.

For CSP-2, the total number of elements was 1028,365, with 619,286 elements in the stationary domain and 409,079 in the rotary domain. At this level, the torque and head results also demonstrated stability, with the variation between successive refinements remaining below 5%. The predicted torque ranged from 1.27 to 1.37 Nm while the head varied

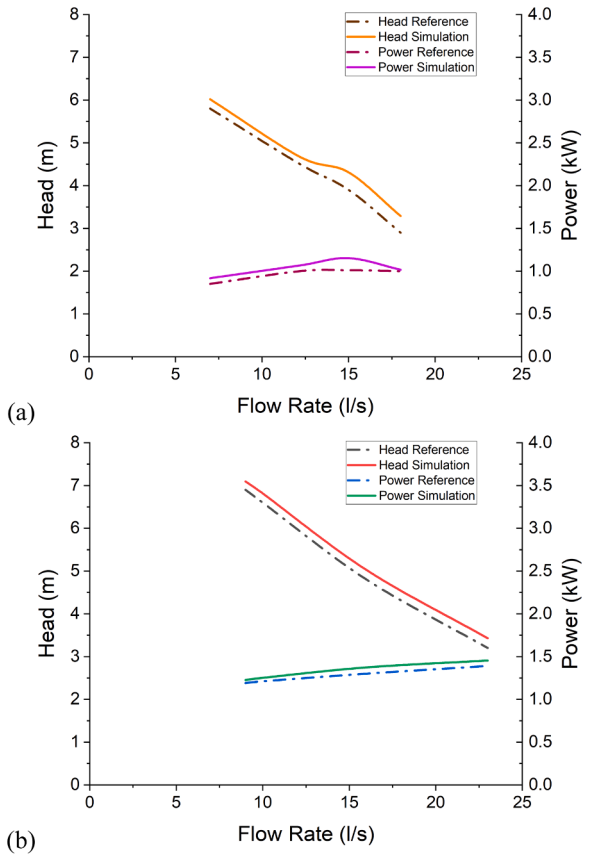

Fig. 11. Validation test results: (a) CSP-1 head and power; (b) CSP-2 head and power.

between 3.4 and 3.39 m under 500 RPM and 10 l/s. This shows that refining the mesh more than the minimum selected size does not lead to significant changes in the performance prediction, while substantially increasing the computational cost. Additionally, for another consideration in checking the mesh quality, the value of y^+in the impeller for both CSP-1 and CSP-2 were observed. For CSP-1, the value of y^+ was 106.53 and for CSP-2 was 71.35. All of the values were in the range of 30–300.

Because of the same mesh topology, turbulence model, and numerical schemes will be employed to all operating conditions, the mesh convergence results at 500 RPM were considered to represent all of the investigated rotational speed range. This approach is commonly adopted in CFD studies for PAT or turbine system [65,66].

3.4. Validation

Validation was carried out by comparing the CFD simulation results of CSPs in pumping mode with the measured performance data provided by the pump manufacturer. This validation aimed to determine whether the modelled geometry and the mesh in the simulation can represent real conditions. Based on the validation tests for both types of the impellers, the CFD results exhibit a similar trend to the manufacturer's data, as shown in Fig. 11.

For CSP-1, the comparison between the simulated pump power and the reference pump power from the manufacturer resulted in a normalised root mean square error (NRMSE) of 6.45%, with an R^2 value of 0.917. When comparing the simulation results with the manufacturer's data for head, the NRMSE was found to be 7.37%, with an R^2 value of 0.995. For CSP-2, using the same parameters, the NRMSE for power was 3.96% with an R^2 value of 0.917, while the NRMSE for head was 4.13% with an R^2 value of 0.995. These errors are primarily attributed to the simulation not accounting for losses in bearings and oil which are captured in the manufacture's performance data. In addition, minor simplifications of the geometry may also have contributed. However, the magnitude of the errors in both models are deemed acceptably small to be reliable for prediction purposes.

4. Numerical results and discussion

4.1. Performance characteristics of CSPAT

Based on the simulation results, the head-flow characteristic of the centrifugal screw PAT in turbine mode for head could be seen in Fig. 12. Fig. 12 demonstrates that increasing the RPM generally leads to higher head values, following the affinity law, which states that head is proportional to the square of rotational speed. This relationship explains the exponential head increase observed with rising RPM. The phenomenon occurs because higher rotational speeds generate greater kinetic energy, producing stronger centrifugal forces that enable higher head generation.

It also reveals that CSP-1 achieves significantly higher heads than CSP-2, particularly at elevated flow rates and rotational speeds. In contrast, CSP-2 maintains more stable head performance progression. This suggests CSP-2 is better suited for more constant flow conditions where stable performance without extreme head variations is required, while CSP-1 proves more appropriate for applications with dynamic head or flow variations.

Based on the data processing from the simulation results, the power generated by the centrifugal screw impeller was obtained. For CSP-1, the power increase relative to rotational speed showed a flatter progression at 300 RPM and 500 RPM, particularly at higher flow rates, compared to at 700 RPM and above. This suggests CSP-1 cannot generate optimal

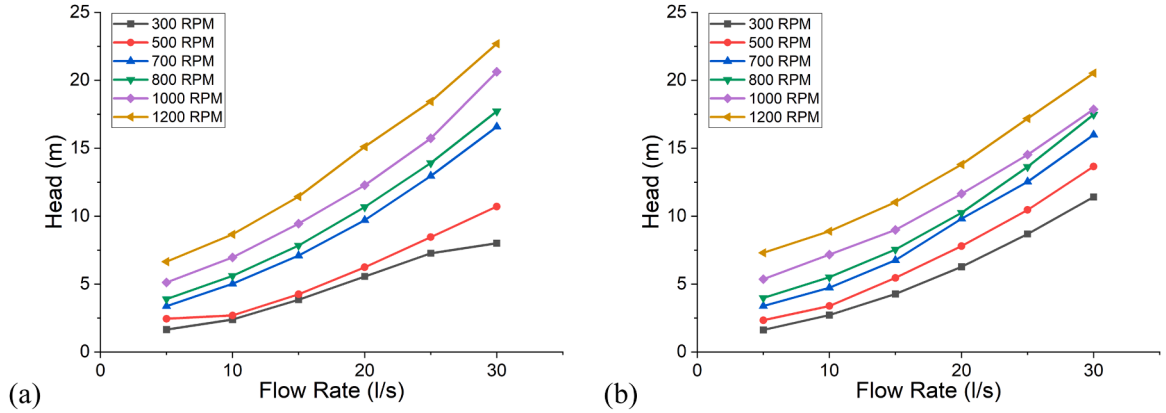

Fig. 12. Head-Flow characteristic curve for CSPAT: (a) CSP-1; (b) CSP-2.

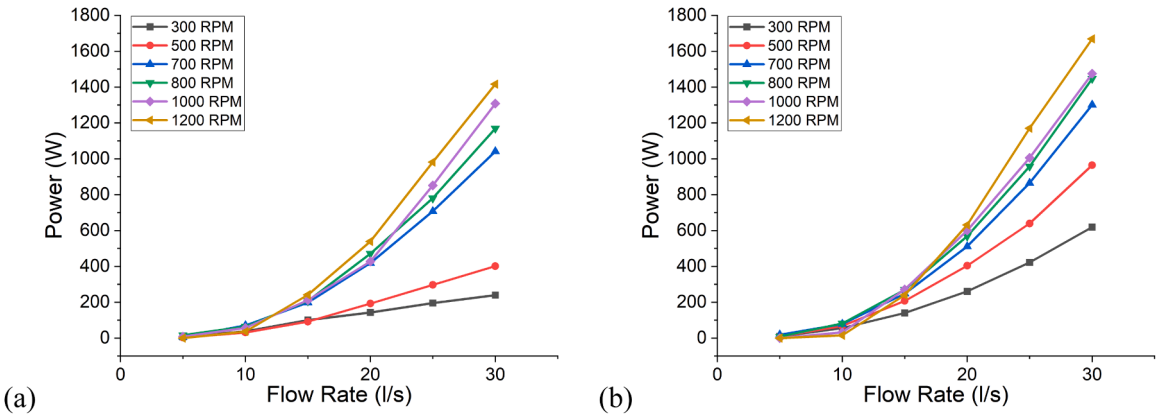

Fig. 13. Power-Flow characteristic curve for CSPAT: (a) CSP-1; (b) CSP-2.

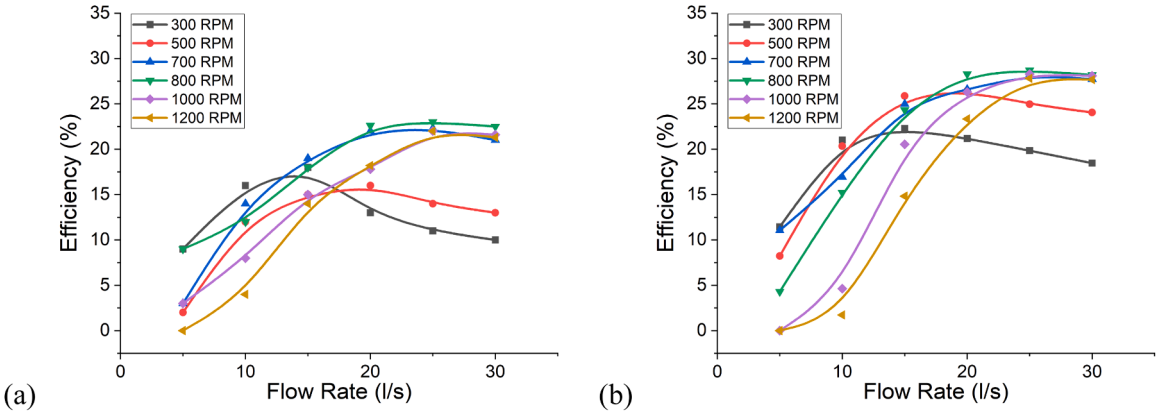

Fig. 14. Efficiency curve CSPAT: (a) CSP-1; (b) CSP-2.

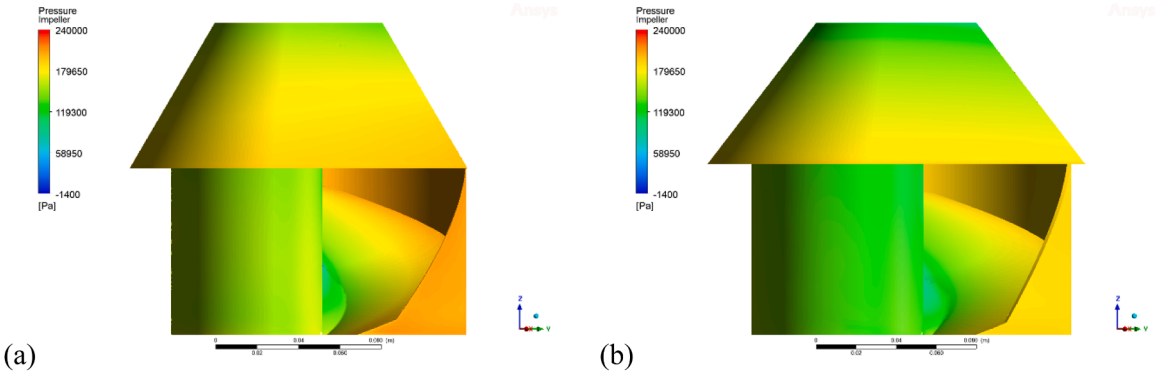

Fig. 15. CSPAT pressure distribution: (a) CSP-1; (b) CSP-2.

power when combining high flow rates with low rotational speeds.

Fig. 13 reveals that CSP-1 generates less power than CSP-2, despite demonstrating higher head values in previous analyses. This performance characteristic suggests CSP-2 achieves higher efficiency in converting both pressure and kinetic energy into mechanical energy. Furthermore, CSP-2 exhibits a more pronounced power increase (steeper gradient) at flow rates exceeding 15 l/s compared to CSP-1. This sharper response indicates CSP-2 operates more optimally than CSP-1 under high-flow conditions.

Based on the simulations and data processing, the centrifugal screw PAT achieved differing peak efficiency at each rotational speed, as seen on Fig. 14. For CSP-1, maximum efficiency of 22.8% was attained at 800 RPM. Beyond the optimal point, a gradual decline in performance was observed.

The maximum efficiency for CSP-1 at 800 RPM was achieved with a flow rate of 25 l/s and head of 13.9 m, producing 780 W of power. Compared to CSP-1, CSP-2 demonstrated higher efficiency due to its larger dimensions, which provided greater impeller surface area for capturing water flow and consequently increased power output. CSP-2 reached its peak efficiency at 800 RPM with 25 l/s flow rate and 13.6 m head, achieving 28.7% efficiency while generating 958 W. CSP-2 also maintained more consistent performance across all rotational speeds and flow rates, particularly between 15–30 l/s. For both CSP-1 and CSP-2, operating above their BEP rotational speeds resulted in decreased efficiency.

Therefore, it can be concluded that enlarging the geometry affects

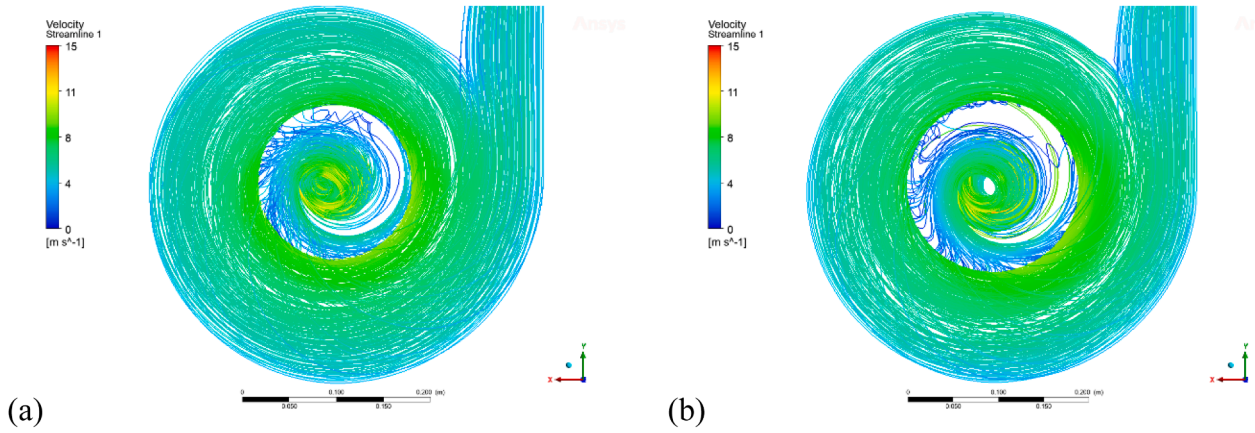

Fig. 16. CSPAT velocity streamline: (a) CSP-1; (b) CSP-2.

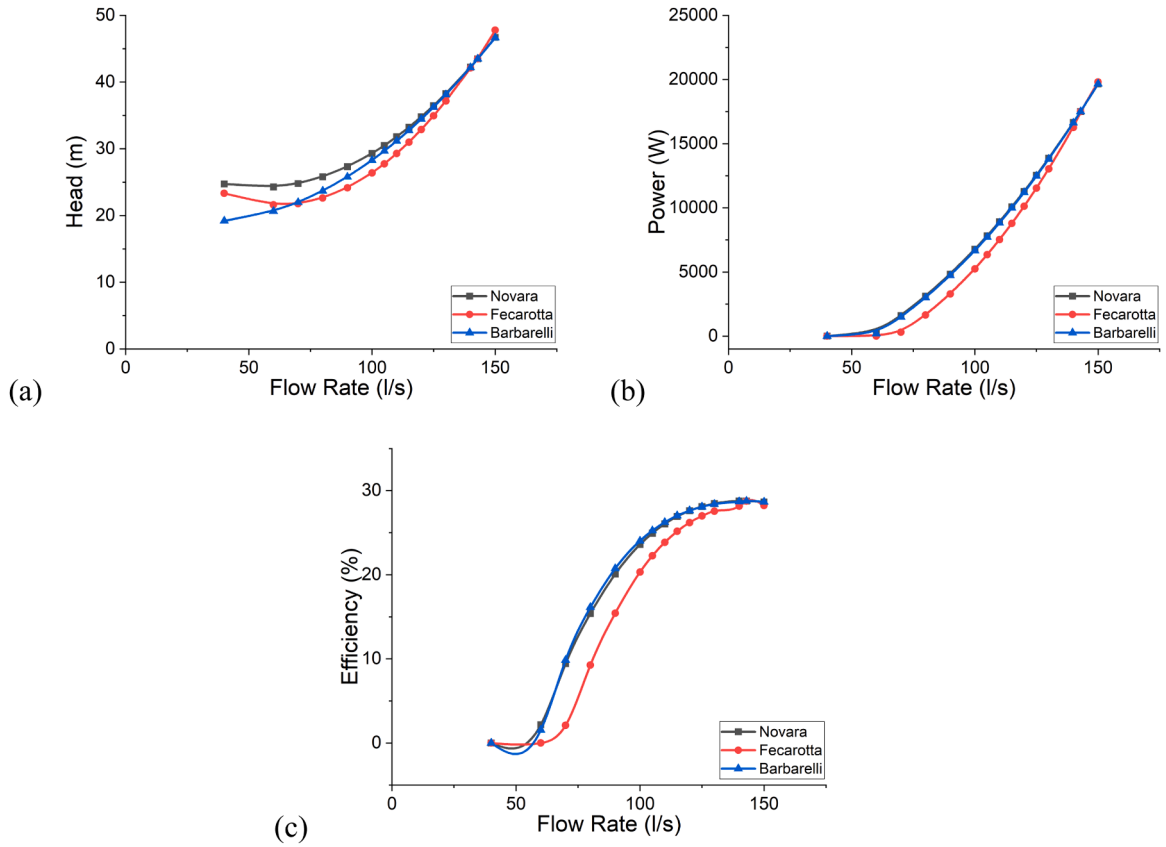

Fig. 17. CSPAT characteristic curves based on existing 1-D analysis for CSP-3: (a) Head; (b) Power; (c) Efficiency.

the performance of the CSPAT. Increasing the impeller dimensions enhances system efficiency, although the improvement remains relatively modest due to the minor size differences between CSP-1 and CSP-2. Both models maintained identical operational flow rates (25 l/s) and comparable head values of 13.9 m for CSP-1 and 13.6 m for CSP-2 at BEP.

The obtained efficiency and power values were relatively low compared to conventional centrifugal pumps of a nearly similar size. Novara et al. [67] conducted a study by installing a conventional centrifugal PAT in Ireland, featuring an impeller diameter of 25 cm, approximately 1.7 times larger than CSP-1 and 1.4 times larger than CSP-2. The study showed that the conventional PAT reached BEP with over 60% mechanical efficiency, at a head of 37.3 m, a flow rate of 15 l/s, a rotational speed of 1520 RPM, and producing up to 2.93 kW of power [67]. The efficiency gap between the CSPATs and the conventional centrifugal PAT at their respective BEPs is significant. The highest efficiency recorded for the CSPAT, which is CSP-2, is approximately 31.3% lower than that of the conventional PAT.

The relatively low efficiency of the CSPAT stems from its unique fish-friendly design featuring a screw-shaped impeller. Unlike conventional centrifugal pumps with curved blades that more efficiently redirect water flow radially outward, the screw impeller cannot utilise and convert water flow into energy as effectively. This demonstrates that the CSPAT experiences a 43–50% efficiency loss compared to conventional centrifugal PATs, which are not designed for fish-friendly operation. This design limitation is further compounded by the CSP's original pumping function configuration, which features bowl-shaped side shrouds designed to capture large water volumes. The screw-type geometry creates its highest-pressure distribution along the outer shroud

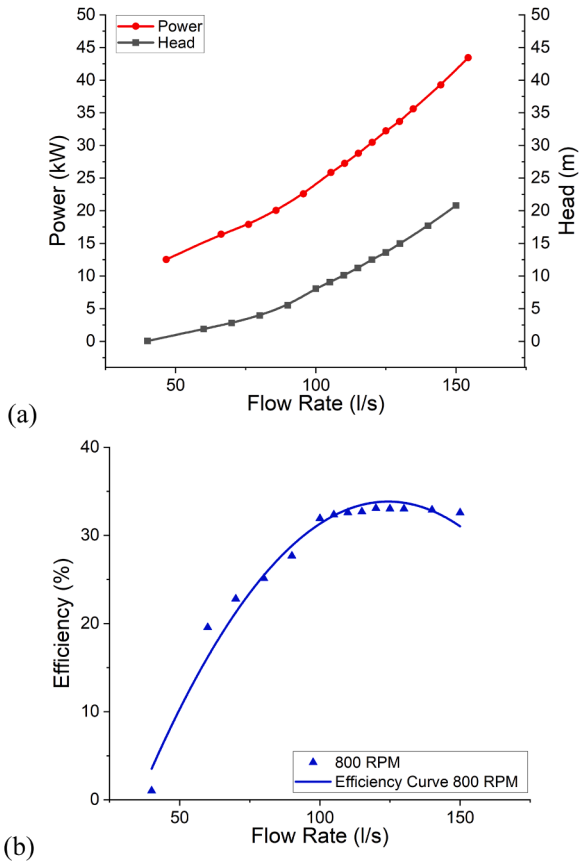

Fig. 18. CSPAT characteristics curves based on CFD analysis for CSP-3: (a) Head and Power; (b) Efficiency.

rather than on the impeller blades (as visualised in Fig. 15). According to fundamental hydraulic principles, this pressure distribution negatively impacts impeller rotation efficiency since maximum power output requires optimal pressure application directly on the blades.

In addition to the pressure distribution, the system's low efficiency and power output are further impacted by swirling flow patterns within the screw impeller (Fig. 16). These swirls create significant pressure fluctuations and can generate vortices and secondary flows. In rotating machinery, especially centrifugal type pumps or turbines, secondary flows and vortices are well known to contribute to hydraulic losses due to additional mixing, shear, and flow instability within passage [68].

Based on the visualization in Fig. 16, the swirl was mainly concentrated along the blade surfaces. Flow rotation close to the blade wall can modify the local pressure field and potentially reduce pressure in certain regions of the blade [69]. The presence of swirl structures of this kind is often associated with a decline in machine performance [70,71]. The streamline plots also revealed a recirculation zone near the blade inlet region, particularly close to the impeller shroud. Similar internal recirculation phenomena have been observed in experimental studies of centrifugal machines [72]. While streamline plots cannot quantify energy loss directly, the appearance of swirl formation generally indicates areas where additional internal dissipation may occur, including in PAT systems [73].

A comparison between CSP-1 and CSP-2 shows that CSP-1 exhibited stronger swirl structures and a wider recirculation region near the blade surfaces. In CSP-2, swirl was still present, but the flow appeared more orderly, and the recirculation region was less extensive. This more stable and consistent internal flow pattern in CSP-2 corresponds well with its higher hydraulic efficiency and power output compared to CSP-1.

4.1.1. Enlarging the CSPAT geometry

Based on the CFD simulation results, the efficiency and power values of both CSP-1 and CSP-2 were relatively low, as shown in Figs. 13 and 14. Therefore, to achieve better performance, a geometric modification was carried out by enlarging the dimensions. This was done to increase the impeller surface area, with the expectation that it would capture more fluid and improve flow conversion. The size enlargement was performed using turbomachinery laws, as shown in the following Eq. (19) [74].

$$\frac{P}{\rho N^3 D^5} = \text{constant} \tag{19}$$

Where P is power (W), ρ is the density of water (998 kg/m^3), N is the rotational speed (rad/s), and D is the diameter (m). To determine the required diameter to achieve higher power output at the same rotational speed, Eq. (19) can be modified by setting the value of *N* as constant, resulting in Eq. (20) as follows:

$$\frac{P_1}{P_2} = \left(\frac{D_1}{D_2}\right)^5 \tag{20}$$

The decision on how much to enlarge the dimensions was based on typical existing MHP potential in Ireland, at existing barriers which could be modified as part of the NRR. This was based on the Hydro Atlas published by the Sustainable Energy Authority of Ireland (SEAI) as well as Inland Fisheries Ireland (IFI). Based on the barriers data, the range of the head of the barriers, especially weirs ranged 0.08 m to 20 m (with over 90% below 10 m). Typical low-head systems in this setting could possess 17.5 kW of gross hydraulic power. The 17.5 kW target was chosen as it represents a practical mid-range output for these typical head conditions, and potential hydropower generated. Using Eq. (20)-Eq. (22), the CSP-3 turbine parameters for 17.5 kW were determined as 31.29 cm for diameter (1.79 × scale-up from CSP-2 reference), with a theoretical H_{tb} of 43.48 m, and the Q_{tb} of 142.91 l/s.

$$\frac{H_1}{H_2} = \left(\frac{D_1}{D_2}\right)^2 \tag{21}$$

$$\frac{Q_1}{Q_2} = \left(\frac{D_1}{D_2}\right)^3 \tag{22}$$

4.2. CSP-3 performance using existing 1D analysis

Based on Eq. (8) through Eq. (15), the performance of CSP-3 is shown in the Fig. 17. Both Novara and Barbarelli methods provide stable changes in values, with head and power increasing steadily in both cases. In contrast, Fecarotta's curve is steeper, and for head, it initially decreases around 40 l/s before rising sharply.

Regarding efficiency, Barbarelli predicts higher efficiency values overall compared to the other two methods, with results not far from Novara's. Fecarotta predicts the lowest efficiency among the three. The highest efficiency reached was estimated to be 28.77%. Theoretically, increasing the dimensions to CSP-3 while keeping the rotational speed constant only results in a small improvement in efficiency compared to the CFD results for CSP-2, despite a relatively significant increase in head and power between CSP-3 and CSP-2.

4.2.1. CSP-3 performance using numerical analysis

Numerical testing was also conducted to evaluate the performance of CSP-3 and to understand phenomena that cannot be explained using 1-D analysis, such as the influence of impeller shape on performance. Based on the numerical analysis from CFD simulations, as shown in Fig. 18, it was found that CSP-3 reaches its BEP condition at a head of 32.2 m, a flow rate of 120 l/s, and a power output of 12.5 kW. This condition achieves an efficiency of 33.08%. In other words, according to the CFD analysis, increasing the dimensions from CSP-2 to CSP-3 while

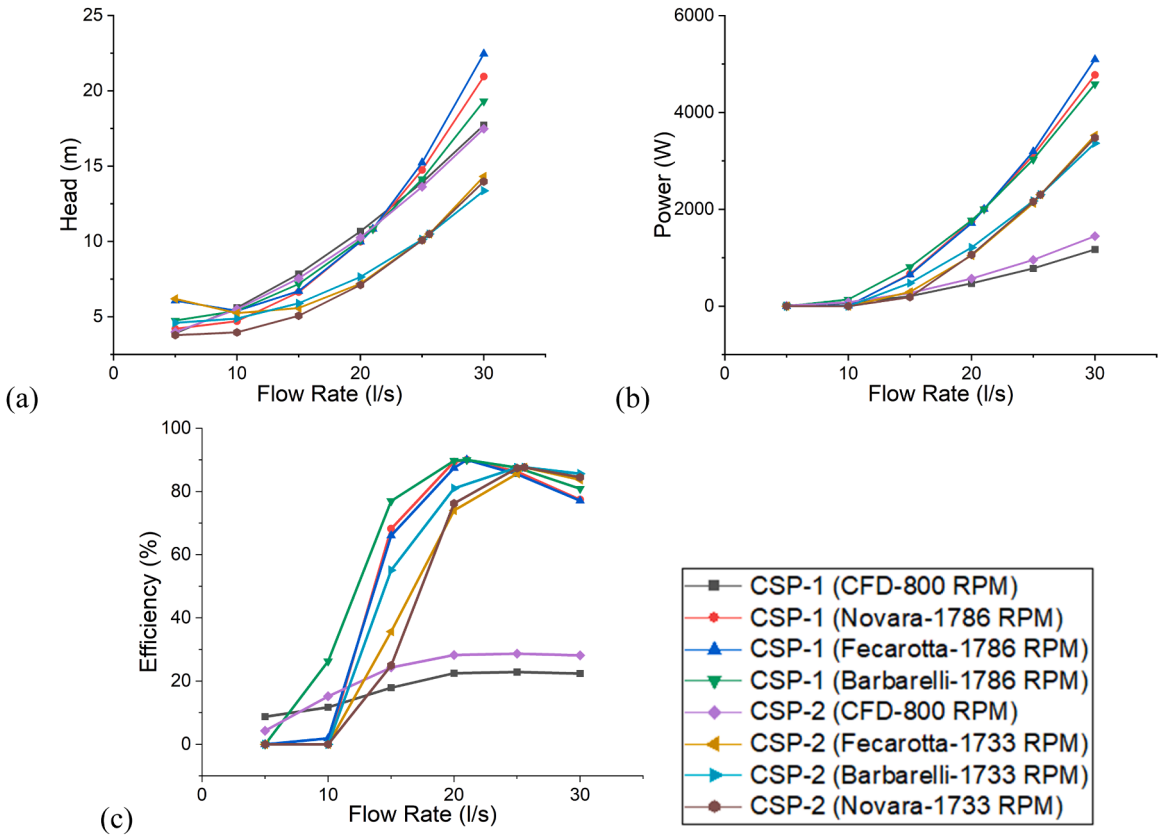

Fig. 19. Comparison of CSPAT characteristic curves for CSP-1 and CSP-2 at BEP based on existing 1-D analysis and CFD results: (a) Head; (b) Power; (c) Efficiency.

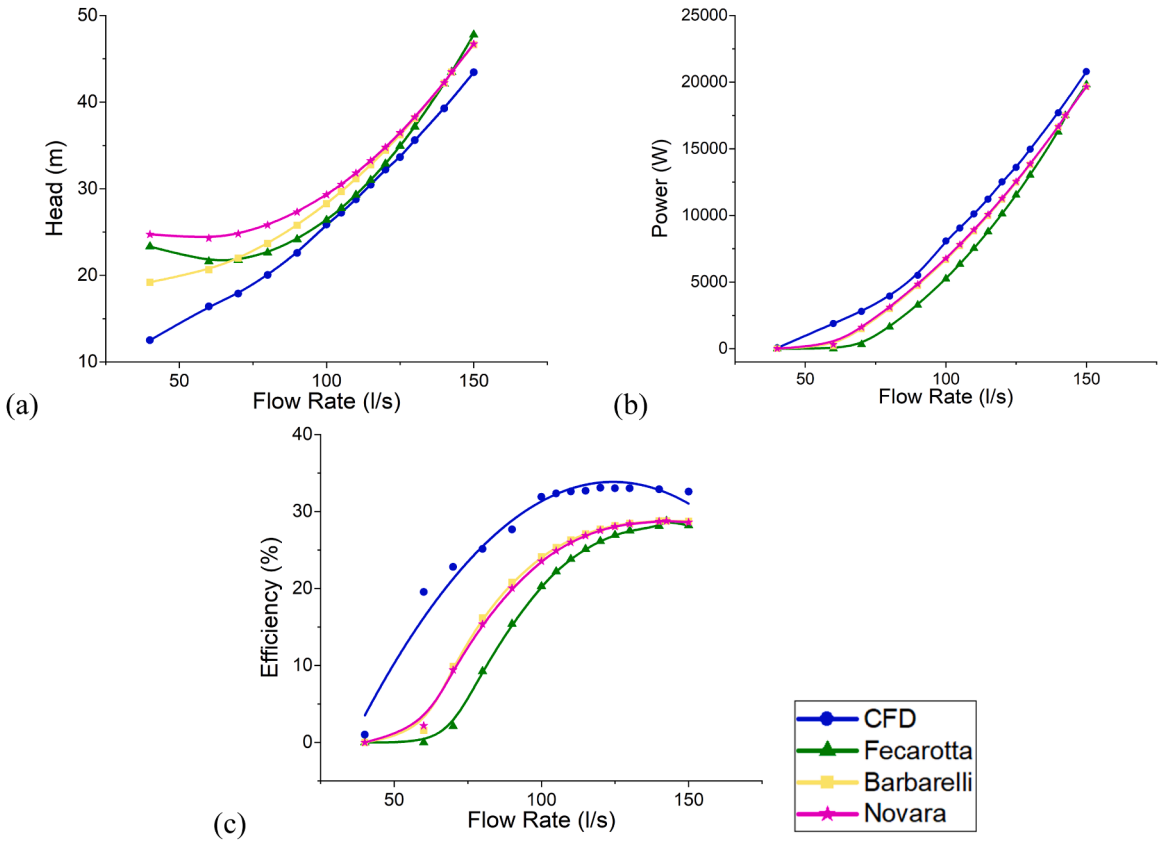

Fig. 20. Comparison of CSPAT characteristic curves for CSP3 at BEP based on existing 1-D analysis and CFD results: (a) Head; (b) Power; (c) Efficiency.

Table 5
Comparison between predicted operating points of CSPAT using the existing and new methods.

	Q_{tb} (l/s)	H_{tb} (m)	P_{tb} (W)	η_{tb}	N_{tb} (RPM)
CSP-1 CFD	25	13.90	779.99	0.228	800.00
CSP-1 New Method	25	14.05	771.05	0.224	800.82
CSP-2 CFD	25	13.60	957.60	0.287	800.00
CSP-2 New Method	24.9	13.47	968.91	0.294	800.52

maintaining the same rotational speed results in an efficiency improvement of 4.38%.

4.3. Comparing 1D analysis and numerical analysis

Obtaining accurate predictions from 1-D analysis is crucial for easy determination the performance of CSPATs in practice. To test this accuracy, prediction results can be compared with field experiments or CFD analysis. In this study, the theoretical predictions are compared with CFD analysis results, which can capture phenomena that theoretical approaches cannot predict. The results for characteristic curves at BEP are shown in Fig. 19 for the comparison between CSP-1 and CSP-2, and in Fig. 20 for the comparison involving CSP-3.

Fig. 19 shows that for CSP-1 and CSP-2, the existing equations differ significantly from the numerical CFD analysis results, especially for the power and efficiency curves. In contrast, for CSP-3, in Fig. 20 the differences between the three existing methods and CFD are not as significant. This indicates that the significant discrepancies mainly arise from the prediction of BEP values when converting from pump BEP to turbine BEP, particularly in power, efficiency, and rotational speed. As a result, the characteristic curve predictions based on BEP values are also affected. For CSP-3, the BEP value used is based on the similarity between the CFD results of CSP-2, so the values are quite similar.

To address this gap, an adjustment is proposed specifically for converting from pump mode BEP to turbine mode BEP for the CSPs.

The analysis uses data from CSP-1 and CSP-2, with pump data provided by the manufacturer, as shown in Table 2, while the turbine data comes from CFD results as discussed in Section 4. The data processing was carried out using Microsoft Excel equipped with Solver and two-variable linear analysis, combining both to minimise error.

From this analysis, the following equations Eqs. (23–26) were derived to predict the operational point of the CSPAT, as presented in Table 5.

$$\frac{Q_{tb}}{Q_{pb}} = -11\eta_{pb} + 7.962 \tag{23}$$

$$\frac{H_{tb}}{H_{pb}} = \frac{1.422}{\eta_{pb}^{1.248}} \tag{24}$$

Table 6
New coefficient values for Eqs. (27 and 28).

Non-dimensional head curve		Non-dimensional power curve	
Coefficients	Values	Coefficients	Values
a	$-0.804b - 0.514c + 0.828$	d	$5.4986\ln N_s - 15.187$
b	$2 \times 10^{10} N_s^{-8.379}$	e	$-6.97\ln N_s + 20.684$
c	$0.0473N_s - 0.6894$	f	$-0.5301N_s^2 + 20.317N_s - 193.78$

$$\frac{N_{tb}}{N_{pb}} = 0.0096\frac{Q_{tb}}{Q_{pb}} + 0.535 \tag{25}$$

$$\frac{P_{tb}}{P_{pb}} = 4.441\left(\frac{N_{tb}}{N_{pb}}\right)^3 \tag{26}$$

The errors from the new equations reached 0.4% for flow rate, 1.07% for head, 0.1% for rotational speed, and 1.18% for power, when compared against CFD results. The CFD model itself was previously validated using laboratory pump experimental data, as shown in Section 3.4. Although these error values are small, there is a potential for overfitting since the dataset used is relatively limited, consisting of only two different pump units, namely CSP-1 and CSP-2.

Meanwhile, to generate equations for predicting the characteristics of CSP, CFD analysis data from CSP-1, CSP-2, and CSP-3 were used, totalling 86 data points. This approach is based on the method by Novara, where both head and power are represented by quadratic equations, with coefficients dependent on the specific speed value. The correlation between relative head and relative power with relative flow rate and specific speed is shown in Fig. 21.

To obtain these equations, IBM SPSS Statistics and Microsoft Excel were used to find equation combinations with high R^2 values and low NRMSE. The analysis produced Eqs. (27 and 28)

$$\frac{H_t}{H_{tb}} = a\left(\frac{Q_t}{Q_{tb}}\right)^2 + b\left(\frac{Q_t}{Q_{tb}}\right) + c \tag{27}$$

$$\frac{P_t}{P_{tb}} = d\left(\frac{Q_t}{Q_{tb}}\right)^2 + e\left(\frac{Q_t}{Q_{tb}}\right) + f \tag{28}$$

Table 7
Comparison of accuracy between the existing and new 1-D prediction methods.

Method	NRMSE Head	R^2 Head	NRMSE Power	R^2 Power
Novara	0.099	0.731	0.067	0.854
Barbarelli	0.076	0.845	0.071	0.836
Fecarotta	0.159	0.315	0.104	0.647
New	0.027	0.979	0.029	0.973

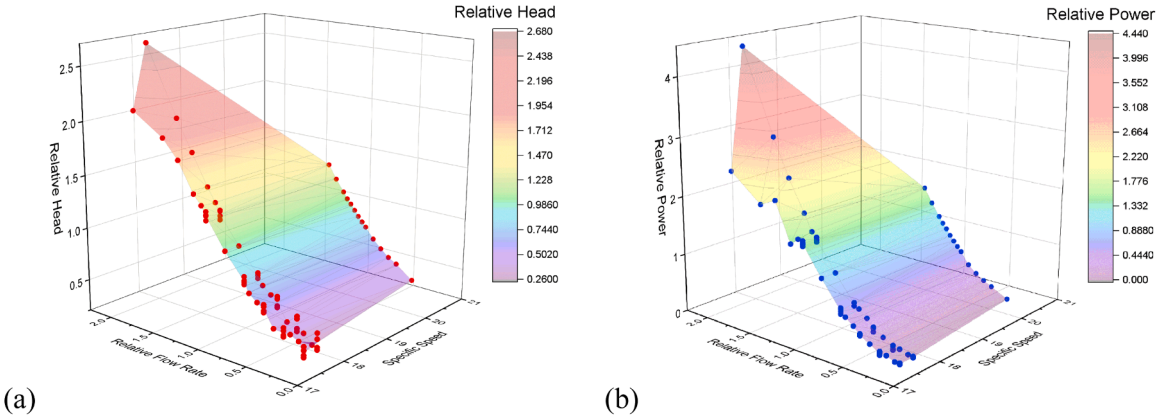

Fig. 21. Relative Characteristic curves of CSPAT to specific speed: (a) Relative head; (b) Relative power.

The coefficient values can be determined based on the correlations shown in Table 6.

When the new equations were tested using BEP values from the CFD results of CSP 1, 2, and 3, they yielded higher R^2 values and lower NRMSE values compared to the three previously existing methods, as shown in the Table 7. These new equations and their error values were developed for specific speeds ranging from 17.5 to 20.5.

However, it should be noted that although the number of data points used to develop the predictive equation is 86, they were all derived from only three pump units. Consequently, the investigated specific speed range is represented by only three discrete values, with limited data density between the lower and upper bounds. This sparse distribution of specific speeds, particularly within the intermediate range, may increase the risk of overfitting and limit the generalisability of the proposed equations.

5. Conclusions

Based on the conducted study, theoretical and numerical approaches have been used to predict the performance and characteristic curves of the CSPs. As an initial step, existing equations from other PAT studies (excluding CSP) were employed to determine the BEP of the CSPAT, based on the BEP of the CSP operating as a pump. Other characteristics were also analysed using available methods from previous studies. These analytical results were compared to the CFD simulations, where significant discrepancies were found, particularly in converting the pump BEP to turbine BEP, especially in power, efficiency, and rotational speed. To validate the CFD results, pump mode simulations were conducted and compared with manufacturer data.

CFD simulations showed that CSP-1 reached an optimum efficiency of 22.8% at a head of 13.9 m and a flow rate of 25 l/s, producing 780 W CSP-2, slightly larger in size, achieved 28.7% efficiency at 13.6 m head and the same flow rate, producing 958 W. Both operated optimally at 800 RPM. To improve CSP performance, a geometric modification was made by enlarging the water inlet diameter to achieve a 17.5 kW power target, based on a national hydropower potential map and average site-head selection. This scaling (CSP-3), analysed through existing 1-D analysis and CFD, showed only minor differences since the similarity basis used was CFD results from CSP-2 as the most efficient design. CFD results for CSP-3 revealed an efficiency increase to 33.1% at a head of 32.2 m and 120 l/s flow rate, generating 12.5 kW at the same speed, 800 RPM.

To obtain more accurate and specific theoretical predictions for CSPs, the simulation results of CSP-1, CSP-2, and CSP-3 were used to develop new equations for predicting BEP values of CSPAT from CSP pump BEP and its performance curves. The prediction error for BEP conversion when compared with CFD result was at most 1.07% (head), 0.4% (flow rate), 0.1% (rotational speed), and 1.18% (power). The latest characteristic prediction equations yielded R^2 of 0.979 for relative head (NRMSE: 0.027), and R^2 of 0.973 for relative power (NRMSE: 0.029). It should be noted that only three pump types with three different specific speeds were used, which may cause overfitting.

Overall, it can be stated that it is possible to adapt and use the CSPs for turbine operation. These proposed equations can be considered as a reference for estimating the BEP and characteristics of the CSPAT system at an early design stage without directly referring to any CFD calculations and experimental investigations.

This approach could potentially benefit developers in making more accurate and faster preliminary investigations during the feasibility analysis of MHP applications. Overall, it reduces uncertainty during the design process of any pump-as-turbine application and improves accuracy in predicting pump-as-turbine performance, making it more suitable for informed decision-making.

Additionally, future research could focus on extending these calculations to a larger set of different sized CSP models. Further testing with more model sizes is necessary to enhance the transferability of these equations and validating them under actual working conditions.

CRediT authorship contribution statement

Naufal Riyandi: Writing – original draft, Visualization, Validation, Methodology, Investigation, Formal analysis, Conceptualization. **John Gallagher:** Writing – review & editing, Visualization, Funding acquisition, Project administration. **Rodolfo Espina-Valdés:** Writing – review & editing, Funding acquisition. **Aonghus McNabola:** Writing – review & editing, Supervision, Project administration, Methodology, Funding acquisition, Conceptualization.

Declaration of competing interest

The authors declare the following financial interests/personal relationships which may be considered as potential competing interests: Naufal Riyandi reports financial support was provided by European Regional Development Fund Interreg Atlantic Area Programme 2021–2027 through the HY4RES project (Hybrid Solutions for Renewable Energy Systems). If there are other authors, they declare that they have no known competing financial interests or personal relationships that could have appeared to influence the work reported in this paper.

Acknowledgements

The authors would like to acknowledge that this research was part funded by the European Regional Development Fund Interreg Atlantic Area Programme 2021–2027 through the HY4RES project (Hybrid Solutions for Renewable Energy Systems) EAPA_0001/2022.

Data availability

The data that has been used is confidential.

References

[1] G.C.D.G. Aubert, Nature Restoration: Contributions to Tackling Climate Change, Iinstitute for European Environmental Policy, 2022 [Online]. Available: https://iep.eu/publications/nature-restoration-contributions-to-tackling-climate-change/.
[2] BORD BIA Irish Food Board, Biodiversity Target Guidance: Pathways to Nature Restoration and Resilience, BORD BIA Irish Food Board, Dubln, 2021.
[3] CIEEM, Rebuilding Nature: Good Practice Guidance for Ecological Restoration, Chartered Institute of Ecology and Environmental Management, Romsey, 2023.
[4] E. Commission, Nature Restoration Regulation, accessed 09 June, https://environment.ec.europa.eu/topics/nature-and-biodiversity/nature-restoration-regulation_en, 2025. accessed 09 June.
[5] E. Commission, Nature Restoration Law, accessed 12 October, https://environment.ec.europa.eu/topics/nature-and-biodiversity/nature-restoration-law_en, 2024. accessed 12 October.
[6] Proposal for a regulation of The European Parliament and of The Council on Nature Restoration [Online] Available: https://eur-lex.europa.eu/resource.html?uri=cellar:f5586441-f5e1-11ec-b976-01aa75ed71a1.0001.02/DOC_1&format=PDF, 2022.
[7] H. King, National Barrier Mitigation Programe, Inland Fisheries Ireland, 2024.
[8] K.P.Z.C.S.J.B.P.M.M.K.-Q.A. McNabola, An Archimedes screw based barrier modification system: synergistic approach to nature restoration and renewable energy generation, in: 41st IAHR World Congress, Singapore, 2025, 22-27 June 2025.
[9] Inland Fisheries Ireland, ed: Inland Fisheries Ireland, 2023.
[10] Global Sustainable Energy Solutions, Micro Hydropower System Design Guidelines, Global Sustainable Energy Solutions, 2020.
[11] D. Tsuanyo, B. Amougou, A. Aziz, B.N. Nnomo, D. Fioriti, J. Kenfack, Design models for small run-of-river hydropower plants: a review, Sustain. Energy Res. 10 (3) (2023) 1–23, https://doi.org/10.1186/s40807-023-00072-1. Springer.
[12] European Union, Directive (EU) 2023/2413 of the European Parliament and of the Council of 18 October 2023 amending Directive (EU) 2018/2001, Regulation (EU) 2018/1999, and Directive 98/70/EC as regards the promotion of energy from renewable sources, and repealing Council Directive (EU) 2015/652, Off. J. Eur. Union L 315/35 (2023).
[13] International Hydropower Association (IHA), Climate Change, International Hydropower Association (IHA), 2024. https://www.hydropower.org/what-we-do/climate-change#:~:text=Hydropower%20is%20the%20oldest%20form,gas%20emissions%20being%20emitted%20annually. accessed 13 March.
[14] E. Brown, S. Sulaeman, R. Quispe-Abad, N. Muller, E. Moran, Safe passage for fish: the case for In-stream turbines, Renew. Sustain. Energy Rev. 173 (2023) 113034, https://doi.org/10.1016/j.rser.2022.113034.

[15] S. Rosenblad, Fish Friendly Turbines for Downstream Migration, Master of Science, Sustainable Development, Environmental Science and EngineeringKTH Royal Institute of Technology, Stockholm, 2023.
[16] EPRI, Chapter 25: Fish-Friendly Turbine Development, EPRI, 2009.
[17] A.T. Piper, P.J. Rosewarne, R.M. Wright, P.S. Kemp, The impact of an Archimedes screw hydropower turbine on fish migration in a lowland river, in: Ecological Engineering, 118, Elsevier B. V, 2018, pp. 31–42, https://doi.org/10.1016/j.ecoleng.2018.04.009.
[18] F. Geiger, P. Rutschmann, U. Stoltz, Measures to improve fish passage through a turbine. Novel Development for Sustainable Hydropower, Springer, Switzerland, 2022 ch. 10.
[19] R. Kumar, A. Abbas, G. Dwivedi, S.K. Singal, Design and cost analysis of fish friendly kaplan tubine: a case study, Mater. Today: Proc. 46 (2021) 5384–5388, https://doi.org/10.1016/j.matpr.2020.08.805.
[20] J. Radinger, R.v. Treeck, C. Wolter, Evident but context-dependent mortality of fish passing hydroelectric turbines, Conserv. Biol. 36 (e13870) (2022), https://doi.org/10.1111/cobi.13870.
[21] T.B. Havn, et al., Downstream migration of Atlantic salmon smolts past a low head hydropower station equippped with Archimedes screw and Francis turbines, Ecol. Eng. 105 (2017) 262–275, https://doi.org/10.1016/j.ecoleng.2017.04.043.
[22] E. Quaranta, A. Bahreini, A. Riasi, R. Revelli, The very low head turbine for hydropower generation in existing hydraulic infrastructures: state of the art and future challenges, Sustain. Energy Technol. Assess. 51 (101924) (2022) 101924, https://doi.org/10.1016/j.seta.2021.101924.
[23] E. Dagdelen, H. Apaydin, Cost-effectiveness of hydroelectric turbines and pumps as an alternative to pressure-reducing valves for electricity production in irrigation lines in Turkey, Water Conserv. Sci. Eng. 9 (59) (2024), https://doi.org/10.1007/s41101-024-00292-6.
[24] D. Mitrovic, J.G. Morillo, J.A.R. Diaz, A.M. Nabola, Optimization-based methodology for selection of pump-as-turbine in water distribution networks: effects of different objectives and machine operation limits on best efficiency point, J. Water Resour. Plan. Manag. 147 (5) (2021).
[25] M. Rossi, M. Renzi, Analytical prediction for evaluating pump-As-turbines (PaTs) performance, Energy Procedia 118 (2017) 238–242, https://doi.org/10.1016/j.egypro.2017.07.011.
[26] X. Sun, H. Huang, Y. Zhao, L. Tong, H. Lin, Y. Zhang, A review ofMethods for "pump as turbine" (PAT) performance prediction and optimal design. Fluid Dynamics & Materials Processing, Tech Science Press, 2025, https://doi.org/10.32604/fdmp.2025.064329.
[27] B.P.M.v. Esch, Fish injury and mortality during passage through pumping stations, J. Fluids. Eng. 134 (071302–1) (2012), https://doi.org/10.1115/1.4006808.
[28] ALDEN Research Laboratory, White Pape - Fish-Friendly Axial Flow Pumps, ALDEN Research Laboratory, Holden, 2015 [Online]. Available, https://www.waterboards.ca.gov/rwqcb9/water_issues/programs/regulatory/docs/appendices/Appendix_J.pdf.
[29] T.H.M. Hoang, U. Shrestha, Y.-D. Choi, Hydraulic and suction performances of the screw centrifugal pump for live fish transfer according to impeller blade inlet shapes, 한국유체기계학회 논문집 25 (1) (2022) 16–25, https://doi.org/10.5293/kfma.2022.25.1.016.
[30] P.H. Patrick, R.S. McKinley, Field evaluation of a hidrostal pump for live transfer of American eels at a hydroelectric facility, N. Am. J. Fish. Manag. 7 (2) (1987) 303–305, https://doi.org/10.1577/1548-8659(1987)7<303:Feoahp>2.0.Co;2.
[31] M.S. White, P.H. Patrick, E. Mason, N. Wiemann, J. Tetreault, Laboratory studies of fish entrainment sampling using a screw centrifugal impeller pump, N. Am. J. Fish. Manag. 43 (3) (2023) 882–888, https://doi.org/10.1002/nafm.10901.
[32] M. Stefanizzi, et al., Development of a 1-D performance prediction model for pumps as turbines, Proceedings 2 (2018) 682, https://doi.org/10.3390/proceedings2110682.
[33] D. Novara, A. McNabola, A model for the extrapolation of the characteristic curves of Pumps as turbines from a datum Best Efficiency point, Energy Convers. Manag. 174 (2018) 1–7, https://doi.org/10.1016/j.enconman.2018.07.091.
[34] S. Derakhshan, A. Nourbakhsh, Experimental study of characteristic curves of centrifugal pumps working as turbines in different specific speeds, Exp. Therm. Fluid Sci. 32 (2008) 800–807, https://doi.org/10.1016/j.expthermflusci.2007.10.004.
[35] S. Barbarelli, M. Amelio, G. Florio, Experimental activity at test rig validating correlations to select pumps running as turbines in microhydro plants, Energy Convers. Manag. 149 (2017) 781–797, https://doi.org/10.1016/j.enconman.2017.03.013.
[36] S.-S. Yang, S. Derakhshan, F.-Y. Kong, Theoretical, numerical and experimental prediction of pump as turbine performance, Renew. Energy 48 (2012) 507–513, https://doi.org/10.1016/j.renene.2012.06.002.
[37] S. Fontanella, O. Fecarotta, B. Molino, L. Cozzolino, R.D. Morte, A performance prediction model for pumps as turbines (PATs), Water. (Basel) 12 (2020) 1175, https://doi.org/10.3390/w12041175.
[38] O. Fecarotta, A. Carravetta, H.M. Ramos, R. Martino, An improved affinity model to enhance variable operating strategy for pumps used as turbines, J. Hydraul. Res. 54 (2016) 332–341, https://doi.org/10.1080/00221686.2016.1141804.
[39] Hidrostal. (n.d.), *The ORIGINAL Screw Centrifugal Impeller Pump*, Hidrostal. [Online]. Available: https://hidrostal.com/Dokumente/Download_190/the-original-screw-centrifugal-impeller-pump-pr0557_en.pdf.
[40] S. Yang, et al., Comparative evaluation of the pump mode and turbine mode performance of a large vaned-voluted centrifugal pump, in: Frontiers in Energy Research, 10, Process and Energy Systems Engineering, 2022, https://doi.org/10.3389/fenrg.2022.1003449.
[41] N. Raman, I. Hussein, K. Palanisamy, B. Foo, An experimental investigation of pump as turbine for micro hydro application, IOP Conf. Ser.: Earth Environ. Sci. 16 (2013) 012064, https://doi.org/10.1088/1755-1315/16/1/012064.
[42] H.K. Versteeg, W. Malalasekera, An Introduction to Computational Fluid Dynamics: The Vinite Volume Method, 2nd ed, Pearson Education Limited, Essex, 2007.
[43] P.J. Roache, Fundamental of Verification and Validation, Hermosa Publisher, New Mexico, 2009.
[44] F.P.V.H.E.C.M.P.-S.P.A. López-Jiménez, Pumps as turbines (PATs) by analysis with CFD models, Int. J. Adv. Sci. Eng. Inf. Technol. 12 (3) (2022).
[45] F. Plua, V. Hidalgo, P.A. Lopez-Jimenez, M. Perez-Sanchez, Analysis of applicability of CFD numerical studies applied to problem when pump working as turbine, Water. (Basel) 13 (2134) (2021) 2134, https://doi.org/10.3390/w13152134.
[46] F.X.E. Vila, CFD Simulations of An Archimedes Screw, Mechanical Engineering, Ostbayerische Technische Hochschule Regensburg, Regensburg, 2019. Bachelor.
[47] S. Purohit, I.F.S.A. Kabir, E.Y.K. Ng, On the accuracy of uRANS and LES-based CFD modeling approaches for rotor and wake aerodynamics of the (New) MEXICOWind Turbine Rotor Phase-III, Energies 14 (5198) (2021) 5198, https://doi.org/10.3390/en14165198.
[48] T.P. Syawitri, Y.F. Yao, B. Chandra, J. Yao, Comparison study of URANS and hybrid RANS-LES models on predicting vertical axis wind turbine performance at low, medium and high tip speed ratio ranges, Renew. Energy 168 (2021) 247–269, https://doi.org/10.1016/j.renene.2020.12.045.
[49] N. Gourdain, Prediction of the unsteady turbulent flow in an axial compressor stage. Part 1: comparison of unsteady RANS and LES with experiments, Comput. Fluids. 106 (2015) 119–129, https://doi.org/10.1016/j.compfluid.2014.09.052.
[50] D. Stefan, M. Rossi, M. Hudec, P. Rudolf, A. Nigro, M. Renzi, Study of the internal flow field in a pump-as turbine (PAT): numerical investigation, overall performance prediction model and velocity vector analysis, Renew. Energy 156 (2020) 158–172, https://doi.org/10.1016/j.renene.2020.03.185.
[51] Q. Pan, D. Zhang, W. Shi, B.P.M. van Esch, Fish damage assessment during the passage through traditional and fish-friendly axial-flow pumps with Lagrangian tracking approach, Ocean Eng. 253 (2022) 111188, https://doi.org/10.1016/j.oceaneng.2022.111188. /06/01/2022.
[52] R.A.B.R.N.M.R.D.K.G.B.V. Vignesh, Comparative study on effective turbulence model for NACA0012 Airfoil using Spalart – Allmaras as a benchmark, Int. J. Trend Sci. Res. Dev. (IJTSRD) 4 (3) (2020).
[53] M.A.A.H.N.A.R.N.M.M.N.M.N.M.N. Dahalan, The evaluation of k-ε and k-ω turbulence models in modelling flows and performance of S-shaped diffuser, Int. J. Automot. Mech. Eng. 15 (2) (2018) 5161–5177, https://doi.org/10.15282/ijame.15.2.2018.2.0399.
[54] D.A.I.M.R.F.N.M. Muhammad, Comparison of standard k-ε and SST k-ωturbulence model for breastshot waterwheel simulation, J. Mech. Sci. Eng. 7 (2) (2020) 39–44.
[55] T.H.M.H.V.A.T.U.S.Y.-D. Choi, Optimization of the meridional plane shape design parameters in a screw centrifugal pump impeller, 한국유체기계학회 논문집 24 (4) (2021) 15–25, https://doi.org/10.5293/kfma.2021.24.4.015.
[56] T.H.M.H.U.S.Y.-D. Choi, Hydraulic and suction performance of the screw centrifugal pump for live fish transfer according to impeller blade inlet shapes, 한국유체기계학회 논문집 25 (1) (2022) 16–25, https://doi.org/10.5293/kfma.2022.25.1.016.
[57] C.M. Jubayern, H. Hangan, Numerical simulation of wind effects on a stand-alone ground mounted photovoltaic (PV) system, J. Wind Eng. Ind. Aerodyn. 134 (2014) 56–64, https://doi.org/10.1016/j.jweia.2014.08.008.
[58] H. Yu, J. Thé, Validation and optimization of SST k-u turbulence model for pollutant dispersion within a building array, Atmos. Env. 145 (2016) 225–238, https://doi.org/10.1016/j.atmosenv.2016.09.043.
[59] ANSYS, Turbulence modeling. Ansys CFX: Training Manual, ANSYS Inc, 2009.
[60] P.F. Koukouvinis, J. Anagnostopoulos, State of the art in designing fish-friendly turbines: concepts and performance indicators, Energies 16 (2023) 2661, https://doi.org/10.3390/en16062661.
[61] M. Rakibuzzaman, S.-H. Suh, H.-H. Kim, Y. Ryu, K.Y. Kim, Development of a hydropower turbine using seawater from a fish farm, Processes 9 (2021) 266, https://doi.org/10.3390/pr9020266.
[62] C. Yang, Q. Zhang, J. Guo, J. Wu, Y. Zheng, Z. Ren, Optimal design and fish-passing performance analysis of a fish-friendly axial flow pump, Appl. Sci. 13 (2023) 12056, https://doi.org/10.3390/app132112056.
[63] B.M. Bierschenk, J. Pander, M. Mueller, J. Geist, Fish injury and mortality at pumping stations: a comparison of conventional and fish-friendly pumps. Marine and Freshwater Research, CSIRO Publishing, 2019, https://doi.org/10.1071/MF18116.
[64] Z. Cao, J. Deng, L. Zhao, L. Liu, Numerical research of pump-as-turbine performance with synergy analysis, Processes 9 (1031) (2021) 1031, https://doi.org/10.3390/pr9061031.
[65] D. Jianguo, G. Chang, D. Adu, R. Darko, M.A.S. Khan, E.O. Antwi, Numerical simulation and computational flow characterization analyses of centrifugal pump operating as turbine, Complexity. 2021 (1) (2021), https://doi.org/10.1155/2021/9695452.
[66] J. Chen, T. Dai, Q. Yang, Effect of rotational speed on performance of mixed flow pump as turbine, Shock Vib. 2021 (2021), https://doi.org/10.1155/2021/6681953.
[67] D. Novara, A. McNabola, Design and year-long performance evaluation of a pump as turbine (PAT) pico-hydropower energy recovery device in a water network, Water. (Basel) 13 (13) (2021) 3014, https://doi.org/10.3390/w13213014.
[68] L. Zhang, L. Kritioti, P. Wang, J. Zhang, M. Zangeneh, A detailed loss analysis methodology for centrifugal compressors, in: Turbomachinery Technical

Conference and Exposition GT2021, 2021, https://doi.org/10.1115/gt2021-59334. Proceedings of ASME Turbo Expo 2021.
[69] L.Z.-L (李子良), H.G. (韩戈), Z.C.-X. (周创鑫), L.X.-G. 卢, Quantitative analysis on influence of secondary flow for centrifugal impeller internal flow, in: Physics of Fluids, 35, AIP Publishing, 2023, https://doi.org/10.1063/5.0139503.
[70] K. Braun, R. Kurz, Analysis of secondary flows in centrifugal impellers, Int. J. Rotating Mach. 2005 (2005) 45–52, https://doi.org/10.1155/IJRM.2005.45. Hindawi.
[71] S. Khullar, K.M. Singh, M.J. Cervantes, B.K. Gandhi, Impact, analysis, and mitigation of flow instabilities in draft tube of Francis turbines, in: Physics of Fluids, 37, AIP Publishing, 2025, https://doi.org/10.1063/5.0247551.
[72] R.W. Westra, L. Broersma, K.v. Andel, N.P. Kruyt, PIV measurements and CFD computations of secondary flow in a centrifugal pump impeller, J. Fluids. Eng. 132 (2010), https://doi.org/10.1115/1.4001803.
[73] L. Xu, et al., A Rortex-based method for evaluating hydraulic losses in pump-turbines: a case study of turbine mode under different load conditions, in: Engineering Applications of Computational Fluid Mechanics, 19, Taylor & Francis, 2025, https://doi.org/10.1080/19942060.2025.2568095.
[74] S.L. Dixon, Fluid Mechanics, Thermodynamics of Turbomachinery, 4th ed, Butterworth-Heinemann, Oxford, 1998.